SOIL MODELS AND VEHICLE SYSTEM DYNAMICS

Ulysses Contreras[1]
Guangbu Li[2]
Craig D. Foster[3]
Ahmed A. Shabana[1]
Paramsothy Jayakumar[4]
Michael D. Letherwood[4]

[1] Department of Mechanical and Industrial Engineering, University of Illinois at Chicago, 842 West Taylor Street, Chicago, Illinois 60607
[2] Department of Mechanical Engineering, Shanghai Normal University, 100 Guilin Road, Shanghai, 200234
[3] Department of Civil and Materials Engineering, University of Illinois at Chicago, 842 West Taylor Street, Chicago, Illinois 60607
[4] U.S. Army RDECOM-TARDEC, 6501 East 11 Mile Road, Warren, MI 48397-5000

Report Documentation Page

Form Approved
OMB No. 0704-0188

1. REPORT DATE	2. REPORT TYPE	3. DATES COVERED
07 MAY 2013	**Technical Report**	**12-06-2012 to 09-04-2013**

4. TITLE AND SUBTITLE **SOIL MODELS AND VEHICLE SYSTEM DYNAMICS**	5a. CONTRACT NUMBER **W56HZV-13-C-0032**
	5b. GRANT NUMBER
	5c. PROGRAM ELEMENT NUMBER
6. AUTHOR(S) **Ulysses Contreras; Guangbu Li; Ahmed Shabana; Paramsothy Jayakumar; Michael Letherwood**	5d. PROJECT NUMBER
	5e. TASK NUMBER
	5f. WORK UNIT NUMBER
7. PERFORMING ORGANIZATION NAME(S) AND ADDRESS(ES) **Department of Mechanical and Industrial Engineering,University of Illinois at Chicago,842 West Taylor Street,Chicago,IL,60607**	8. PERFORMING ORGANIZATION REPORT NUMBER **; #23850**
9. SPONSORING/MONITORING AGENCY NAME(S) AND ADDRESS(ES) **U.S. Army TARDEC, 6501 East Eleven Mile Rd, Warren, Mi, 48397-5000**	10. SPONSOR/MONITOR'S ACRONYM(S) **TARDEC**
	11. SPONSOR/MONITOR'S REPORT NUMBER(S) **#23850**

12. DISTRIBUTION/AVAILABILITY STATEMENT
Approved for public release; distribution unlimited

13. SUPPLEMENTARY NOTES

14. ABSTRACT

The mechanical behavior of soils may be approximated using different models that depend on particular soil characteristics and simplifying assumptions. For this reason, researchers have proposed and expounded upon a large number of constitutive models and approaches that describe various aspects of soil behavior. However, there are few material models capable of predicting the behavior of soils for engineering applications and are at the same time appropriate for implementation into finite element (FE) and multibody system (MBS) algorithms. This paper presents a survey of some of the commonly used continuum-based soil models. The aim is to provide a summary of continuum-based soil models and examine their suitability for integration with the large-displacement FE absolute nodal coordinate formulation (ANCF) and MBS algorithms. Special emphasis is placed on the formulation of soils used in conjunction with vehicle dynamics models. The implementation of these soil models in MBS algorithms used in the analysis of complex vehicle systems is also discussed. Because semi-empirical terramechanics soil models are currently the most widely used to study vehicle/soil interaction, a review of classical terramechanics models is presented in order to be able to explain the modes of displacements that are not captured by these simpler models. Other methods such as the particle-based and mesh-free models are also briefly reviewed. A Cam-Clay soil model is used in this paper to explain how such continuum-mechanics based soil models can be implemented in FE/MBS algorithms.

15. SUBJECT TERMS
Soil mechanics; Finite element; Multibody systems; Terramechanics.

16. SECURITY CLASSIFICATION OF:			17. LIMITATION OF ABSTRACT	18. NUMBER OF PAGES	19a. NAME OF RESPONSIBLE PERSON
a. REPORT **unclassified**	b. ABSTRACT **unclassified**	c. THIS PAGE **unclassified**	**Public Release**	**94**	

Standard Form 298 (Rev. 8-98)
Prescribed by ANSI Std Z39-18

ABSTRACT

The mechanical behavior of soils may be approximated using different models that depend on particular soil characteristics and simplifying assumptions. For this reason, researchers have proposed and expounded upon a large number of constitutive models and approaches that describe various aspects of soil behavior. However, there are few material models capable of predicting the behavior of soils for engineering applications and are at the same time appropriate for implementation into finite element (FE) and multibody system (MBS) algorithms. This paper presents a survey of some of the commonly used continuum-based soil models. The aim is to provide a summary of continuum-based soil models and examine their suitability for integration with the large-displacement FE *absolute nodal coordinate formulation* (ANCF) and MBS algorithms. Special emphasis is placed on the formulation of soils used in conjunction with vehicle dynamics models. The implementation of these soil models in MBS algorithms used in the analysis of complex vehicle systems is also discussed. Because semi-empirical terramechanics soil models are currently the most widely used to study vehicle/soil interaction, a review of classical terramechanics models is presented in order to be able to explain the modes of displacements that are not captured by these simpler models. Other methods such as the particle-based and mesh-free models are also briefly reviewed. A Cam-Clay soil model is used in this paper to explain how such continuum-mechanics based soil models can be implemented in FE/MBS algorithms.

Keywords: Soil mechanics; Finite element; Multibody systems; Terramechanics.

1. INTRODUCTION

There are a number of situations in which a vehicle may need to traverse an unprepared terrain. It may happen that the only viable means of reaching a desired objective is through an off-road route. In such an instance, it would be desirable to have an understanding of how a vehicles design affects its performance in such an environment. Often, vehicles are specifically designed for off-road usage. This is the case for military, construction, and agriculture vehicles as well as unmanned/manned rovers. In all cases it is important to be able to predict (to varying degrees) the conditions under which a vehicle may become incapacitated due to loss of traction. There are other vehicle-terrain related effects that might need to be modeled. For instance, in the case of agricultural vehicles, it is important to be able to predict the compaction induced in the soil. Soil compaction has been determined to cause a reduction in crop yield. It is thus important to minimize a vehicles impact on the terrain. Terramechanics is the field tasked with producing the tools necessary to model the vehicle-terrain interaction over unprepared terrain.

Over the past decades, there have been a number of vehicle terrain interaction studies published which explicitly treat the simplified vehicle dynamic equations of motion together with the semi-empirical equations for the soil. One of the recent trends is the incorporation of semi-empirical terramechanics equations or the co-simulation of finite element (FE) soil models with MBS environments. These environments provide a framework in which the dynamic interaction between vehicle and terrain may be modeled. Incorporation of FE soil within multibody system algorithms can provide a higher fidelity simulation of the dynamic vehicle-terrain interactions. The integration of these FE soil models with MBS algorithms for modeling vehicle/soil interaction represents a challenging implementation and computational problem that

has not been adequately covered in the literature. This integration is necessary in order to be able to develop a more detailed and a more accurate vehicle/terrain dynamic interaction models.

The ability to capture the soil behavior modeled under dynamic loading conditions is of particular interest in the FE/MBS approach to terramechanics. The mechanical characteristics of soils, as with any other material, depend on the loading and soil conditions.

The mechanical characteristics of soils, as with any other material, depend on the loading and material state. The response of the soil model to loading conditions depends on the assumptions used in and the details captured by the specific model. Some approximations are based on simple discrete elastic models that do not capture the distributed elasticity and inertia of soil. More detailed soil models employ a continuum mechanics approach that captures the soil elastic and plastic behaviors. Continuum mechanics-based soil models can be implemented in finite element (FE) algorithms. Nonetheless, the integration of these FE soil models with multibody system (MBS) algorithms for modeling vehicle/soil interaction represents a challenging implementation and computational problem that has not been adequately covered in the literature. This integration is necessary in order to be able to develop more detailed and more accurate vehicle/terrain dynamic interaction models.

1.1 Complexity of Soil Modeling

Depending on the level of detail that needs to be considered in a soil investigation, the parameters that define the soil in a computer model can significantly vary. However, among the many different characteristics of soil behavior, there are a few that must be considered in a soil model suitable for integration with FE MBS environments. These characteristics are summarized as follows:

1. **Shear strength and deformation characteristics**: The mean stress and change in volume produced by shearing greatly affects the shear strength and deformation characteristics of soil. Soils generally exhibit higher shear strength with increasing mean stress (applied pressure) due to interlocking effects. At very high mean stresses, however, soils may fail or yield due to pore collapse, grain crushing, or other phenomena. The dilatation of soil under shear loading is shown in Figure 1b as adapted from [1,2]. Sand demonstrates interlocking behavior that increases with a corresponding increase in the density of soil.
2. **Plasticity**: An increase of applied stress beyond the elastic limit results in an irrecoverable deformation which often occurs without any signs of cracking or failure. A small elastic region which results in plastic behavior at or near the onset of loading is characteristic of many soils.
3. **Strain-hardening/softening**: This soil characteristic can be defined as change in the size, shape, and location of the yield surface. This can be identified graphically as shown in Figure 1 [2]. The dilatation of dense granular material, such as sand, and over-consolidated clays is commonly associated with the strain-softening behavior. Likewise, the compaction of loose granular material, such as sand, and normally consolidated clays is commonly associated with the strain-hardening behavior (Figure 1).

Other characteristics of soil such as temperature dependency, etc. are not considered here because they are beyond the scope of this review paper.

The complexities involved in modeling soil stem from the anisotropy, inhomogeneity, and nonlinear material response of soil. Confounding the situation more is that a standard set of material parameters have not been chosen for characterization of soil. Also, a single all-

encompassing soil model has not been produced and may not be produced in the near future. The geotechnical engineer has at his disposal countless numbers of soil models all with different areas of applicability. The terramechanicist must pick through these models to find those which are suitable for integration with finite element and MBS environments.

1.2 Objective and Scope of this Paper

This paper aims to review some of the existing basic terramechanics and continuum mechanics-based soil models and discuss their suitability for incorporation into FE/MBS simulation algorithms. The main goal is to review continuum soil models that have the potential to be integrated with MBS vehicle models. The paper also discusses how this FE soil/MBS vehicle integration can be achieved. It is important to point out that the goal of this paper is not to review all geotechnical soil mechanics models or provide a comprehensive review of standard or classical terramechanics models. There are several excellent review articles on these two topics. The objective of this review paper is to address problems associated with the use of continuum-based soil models in the area of vehicle/soil interaction. The literature is weak in this area as evident by the small number of investigations that are focused on the use of continuum-based soil models in the study of the vehicle/terrain interaction. Nonetheless, since semi-empirical terramechanics models are the most widely used, a review of these models is appropriate to make clear the basic differences between terramechanics and continuum-based soil models. This also applies to the mesh-free and discrete element methods which are reviewed briefly to give an explanation of what they are and distinguish them from the continuum-based soil models. Therefore, the intention is not to provide a comprehensive review of terramechanics or continuum-based soil models or other methods, but to focus on continuum-based FE soil models

that can be integrated with MBS vehicle algorithms. The review presented in the paper clearly shows a weakness of the literature in this area, as evident by the following facts:

1. The weakness of the literature on continuum-based soil models for vehicle/soil interaction is evident by the small number of investigations on this important topic. The authors attempted to cite most papers in this area. This weakness in the literature is attributed to the problems and challenges encountered when developing accurate continuum-based soil models that can be integrated with detailed MBS vehicle models.
2. Most of the investigations that employ continuum-based soil models in vehicle dynamics are based on a *co-simulation approach* that requires the use of two different computer codes; a finite element code and a MBS dynamics codes. This is also the approach which is used when FE models are used for tires. The co-simulation approach allows only for exchanging state and forces between the two codes; but does not allow for a unified treatment of the algebraic constraint equations that must be satisfied at the position, velocity, and acceleration levels in the MBS algorithms.
3. This paper proposes a method that can be considered as a departure from the co-simulation approach (Sections 6 and 7). ANCF finite elements can be used for both tires and soils and can be integrated with MBS algorithms. While the concern that a detailed ANCF model may lead to significant increase of the CPU time is a valid concern, it is important to realize that the models with significant details that are currently being simulated were un-imaginable to simulate a decade ago. ANCF models with significant details are becoming computationally feasible, unlike DEM models which are still out of the range of possibility. Models being simulated today were not

computationally feasible a decade ago. The concerns with regard to the use of ANCF finite elements for soil and tire modeling are addressed in Section 7 of this paper.

4. All commercial MBS computer codes do not have the capability of modeling continuum-based soils. These codes are not designed for large deformations and do not allow for the use of general constitutive equations when structural finite elements are used. This paper aims at addressing this deficiency as part of its objective and critical analysis.

1.3 Organization of the Paper

This paper is organized as follows. Section 2 outlines the empirical, analytical, semi-empirical, and parametric approaches used in terramechanics. Together, in this manuscript, these are referred to as the classical or standard terramechanics approaches. Also reviewed are some of the tools and methodologies which determine the parameters used in the definitions of the terramechanics models. Section 3 describes the continuum mechanics based soil models. These models include elastic-plastic, viscoplastic, and bounding surface plasticity formulations. Section 4 describes three of the most popular particle-based and meshfree methods; the discrete element method, smoothed particle hydrodynamics, and reproducing kernel particle method. The current research interests of the authors emphasize FE based soil/MBS methods. Section 5 offers a comparison of the various soil models presented in the previous sections and a suitable soil model for implementation in a FE/MBS algorithm is selected. The ANCF computer implementation and the use of ANCF kinematics to predict basic continuum-based soil deformation tensors are outlined in Section 6. Section 7 describes the procedure for the incorporation of the selected soil model with an ANCF/MBS formulation. The structure of the dynamic equations that allows for systematically integrating soil models with FE/MBS system

algorithms used in the virtual prototyping of vehicle systems is presented. Section 8 offers a summary and describes the direction of future work.

2. TERRAMECHANICS-BASED SOIL MODELS

Terramechanics is the study of the relationships between a vehicle and its environment. Some of the principal concerns in terramechanics are developing functional relationships between the design parameters of a vehicle and its performance with respect to its environment, establishing appropriate soil parameters, and promoting rational principles which can be used in the design and evaluation of vehicles [3]. The standard parameters by which vehicle performance is compared include drawbar-pull, tractive efficiency, motion resistance, and thrust. If the normal and shear stress distributions at the running gear-soil interface are known, then these parameters are completely defined. The following subsections review some of the more common terramechanics models suitable for implementation in a MBS environment.

2.1 Empirical Terramechanics Models

One approach used to establish the appropriate parameters, properties, and behaviors of soil involves the determination of empirical relationships based on experimental results which can be used to predict at least qualitatively the response of soils under various conditions [4]. Concerns were raised as to whether the relationships established by this method could be applied in circumstances which were entirely dissimilar to those in which they were established [4]. Bekker proposed using only experiments that realistically simulated the manner in which the running gear of a vehicle traversed the terrain. This entailed using soil penetration plates comparable in size to the contact patch of a tire (or track), and producing pressures and shear forces of comparable magnitude to those produced by a vehicle. Parametric models, which are based on

experimental work and have been widely used, offer practical means by which an engineer can qualitatively evaluate tracked vehicle performance and design. Using these principles, Bekker developed the *Bevameter*. When a tire or a track traverses a terrain, soil is both compressed and sheared. A Bevameter measures the terrains response to normal and shear stresses by the application of penetration plates and shear heads. These responses are then used to produce pressure-sinkage and shear stress-shear displacement curves. These curves are then taken as characteristic response curves for each type of terrain.

Another terrain characterization device of importance (due to its widespread use) is the *cone penetrometer*. A penetrometer applies simultaneously shear and normal stresses. A simplified version of a penetrometer can be visualized as a long rod with a right circular cone on one end. Penetrometers are pushed (at a certain rate) into the soil and the resulting force per unit cone base area, called the *cone index* (CI), is measured. These cone indices can then be used to establish the *trafficability*, on a one or fifty pass basis, of vehicles in different types of terrain [5]. Trafficability is the measure of a vehicle's ability to traverse terrain without becoming incapacitated. Hence, a vehicle with a CI on a fifty pass basis can be expected to make fifty passes on a particular route without becoming incapacitated. It is important to note that individual soil parameters cannot be derived from cone penetration tests. It has been established that the cone penetrometer measures different terrain properties in combination and it is impossible to determine to what degree each particular property affects the results of cone penetrometer tests [5].

A collection of data (CI, Vehicle Cone Index, Rating Cone Index, etc.) and algorithms used to predict vehicle mobility on terrain specific to certain parts of the world, as compiled beginning in the late 1970's, is referred to as the *NATO Reference Mobility Model* (NRMM).

Using the NRMM, the cone penetrometer and the cone index derived from it can be used on a "go/no go" basis of vehicle trafficability in a variety of terrains around the world. While the use of the cone index and the NRMM for *in situ* measurement of soil strength for use in decision making is invaluable, the empirical method is not suited for vehicle development, design, and operation purposes [6]. Design engineers require the use of vehicle parameters which are simply not taken into consideration in the empirical methods.

2.2 Analytical and Semi-Empirical Terramechanics Models

Purely analytical terramechanics models inadequately capture the interaction between the tire and soil interface. For this reason, semi-empirical approaches are more common. Soils modeled as elastic media can be used to predict the stress distribution in the soil due to normal loads. Figure 2 gives a depiction of the formula used to define the stress a at point R units away from the point of application of the load. The resulting equation for the normal stress at a point is called the *Boussinesq equation* and is given below [4].

$$\sigma_z = \frac{3W}{2\pi R^2}\cos^3\theta \tag{1}$$

where W is the magnitude of the point load applied at the surface, R is radial distance at which the stress is being calculated, and θ is the angle between the z axis and the line segment for R. Notice that the Boussinesq equation does not depend on the material; it gives the stress distribution for a homogeneous, isotropic, elastic medium subject to a point load on the surface [4]. Once the stress distribution for a point load is known, then, given the contact area one may integrate the point load stress formula over the contact area to determine the normal stress distribution in the soil. For an evenly distributed load applied under a circular loading area, as

shown in Figure 3, one can show that integrating the Boussinesq equation over the contact area leads to

$$\sigma_z = 3p_0 \int_0^{r_0/Z} \frac{u\ du}{\left(1+u^2\right)^{5/2}} = p_0 \left[1 - \frac{Z^3}{\left(Z^2+r^2\right)^{3/2}} \right] \tag{2}$$

Where the variables for the above equation are defined as in Figure 3, and $u^2 = \left(r/z\right)^2$. For a contact strip (shown in Figure 4), which may be taken as the idealization of the contact area under a track, one can show that the equations for the stresses at a point are

$$\left.\begin{aligned} \sigma_x &= \frac{p_0}{\pi}\left(\theta_2 - \theta_1 + \sin\theta_1\cos\theta_1 - \sin\theta_2\cos\theta_2\right) \\ \sigma_z &= \frac{p_0}{\pi}\left(\theta_2 - \theta_1 - \sin\theta_1\cos\theta_1 + \sin\theta_2\cos\theta_2\right) \\ \tau_{xz} &= \frac{p_0}{\pi}\left(\sin^2\theta_2 - \sin^2\theta_1\right) \end{aligned}\right\} \tag{3}$$

These equations are derived with the assumptions that the contact patch is an infinitely long strip with constant width, the track links are rigid, and a uniform pressure is applied (see Figure 4 for definition of variables). Models based on the theory of elasticity which do not take into account the effect of plastic deformations cannot, in general, be used to predict the shear stress distribution at the soil-tire interface. Another shortfall of these elasticity models is that they may not be applied when loads become too large.

The most widely known methods for semi-empirical analysis of tracked vehicle performance are based on the developments initiated by Bekker. Bekker's pressure-sinkage equations, and its modifications, are now widely used in track-terrain interaction studies. For examples of such studies refer to Ryu et al. [7], Garber and Wong [8], Okello [9,10], Rubinstein and Coppock [11], Park et al. [12]. Similarly for tire-terrain interactions see, among others, Mao

and Han [13], Sandu et al. [14], Schwanghart [15]. A modified Bekker's pressure sinkage relationship is given by [3]

$$z_0 = \left(\frac{p}{\left(k_c/b\right) + k_\phi} \right)^{1/n} = \left(\frac{W/bl}{\left(k_c/b\right) + k_\phi} \right)^{1/n} \tag{4}$$

In this equation, z_0 is the sinkage, p is the pressure, W is magnitude of the applied load, b is contact depth, l is the contact patch length, k_c and K_ϕ are the pressure-sinkage parameters for the *Reece equation* [16]. This pressure-sinkage relationship together with a criterion for shear failure (most often the Mohr-Coulomb failure criteria) can be used to predict the performance of the vehicle.

A variety of pressure-sinkage relationships exist; these pressure sinkage models attempt to capture and correct for behavior that was not considered in the original formulation. Response to cyclic loading, addition of terms that capture the rate effect of loading, the use of elliptical contact areas, and the extension to small diameter wheels are examples of some of the modifications made to the pressure sinkage formulation. An example of a recently published modification to the pressure-sinkage formulation is that proposed by Sandu et al. [17]. The uncertainty in the terrain and moisture content is incorporated into the pressure-sinkage and shear-displacement relations to allow for the propagation of uncertainty in the model. This polynomial chaos approach can efficiently handle large uncertainties and can simulate systems with high nonlinearities. In the proposed model, the moisture content is written as

$$m = \sum_{j=1}^{S} m^j \psi\left(\xi\right)^j \tag{5}$$

where S is the number of terms in the expansion, m^j is the jth moisture content proportionality factor, $\psi\left(\xi\right)^j$ are orthogonal polynomials, and ξ is a random variable. This moisture content

formulation is then used to model the propagation of uncertainty in the pressure-sinkage and shear-displacement relations using the collocation method. The resulting substitution gives the stochastic pressure-sinkage and stochastic shear-displacement relations.

As another example, recent work has been directed at capturing the manner in which grousers on tracked vehicles affect terrain. The oscillations seen in the experimental pressure-sinkage plots caused by grousers can be captured by enhancing the pressure–sinkage relationship with a dynamic term as follows [18]:

$$p(z) = \left(ck_c' + \gamma b k_\phi'\right)\left(\frac{z}{b}\right)^n + A\sin\left(\omega t + \Phi\right) \tag{6}$$

where the parameters in the equivalent standard Bekker's equation are defined as above, A is the amplitude of the oscillation, t is time, ω is the frequency at which the oscillations occur, and Φ is an optional phase shift that can be applied to the model for fitting the simulation predictions to experimental data or applying a correction to account for the initial orientation of the grousers. Dynamic terramechanics models of this sort offer a better approximation of soil response to effects caused by grousers.

Other semi-empirical models have been proposed by Wong [3] including the NTVPM, RTVPM, and NWVPM models. Wong's models are based on the design parameters of vehicles and an idealization of the track terrain interface. These idealizations, for the case of the flexible track NTVPM model, can be seen in Figure 5. With this configuration and variable definitions, the following pressure-sinkage relationship was given [3]:

$$Z_{li+1} = Z_{ai} - \frac{T}{Rk_u} + \sqrt{\left(Z_{ai} - Z_{ri}\right)^2 + \frac{2T}{Rk_u}\left[\frac{T}{2Rk_u} - Z_{ai} + R\cos\varphi_{ri} + Z_{ci+1}\right]} \tag{7}$$

where Z_{li+1} is the sinkage at point F shown in Figure 5, T is the tension in the track per unit width, R is the radius of the road wheel, and k_u and φ_{ri} are modal parameters. Z_{ai}, Z_{ri}, and Z_{ui} are the sinkage of road wheel i at points A, B, and C respectively. The associated shear-displacement relationship is given by

$$s(x) = \left(c + p(x)\tan\varphi\right)\left[1 - \exp\left(-\frac{\left(l - (1-i)x\right)}{K}\right)\right] \tag{8}$$

where $p(x)$ is the normal pressure on the track at x, l is the distance between the point at which shearing begins and the corresponding point on the track, i is the slip, K is the shear deformation parameter, and c and φ are the Mohr-Coulomb failure criteria parameters. Experimental and semi-empirical terramechanics models tend to be simple and do not capture many modes of the soil deformations that can be captured using the more general continuum mechanics-based soil models.

3. CONTINUUM MECHANICS-BASED SOIL MODELS

A large number of continuum soil models have been proposed in the literature, however, as previously mentioned, the focus of this investigation is not to present a comprehensive review of the soil models. The focus is mainly on soil models which have the potential for integration with MBS vehicle models. We discuss the basic framework for such models and some of the more common models. Most of these models are suited for implementation in a finite element framework, as will be discussed in Sections 6 and 7. These continuum-based soil models are briefly reviewed in this section; starting in Section 3.1 with the theory of elastoplasticity which is a framework for developing material models. The subsequent subsections present soil models that fall within this framework and its extensions.

3.1 Theory of Elastoplasticity

Given that soils typically experience both recoverable and non-recoverable deformation under loading, elastoplastic theory and several augmentations of the theory have been widely applied to soils. Elastoplasticity theory is based on the decomposition of the strain into elastic and plastic parts. In the case of small strains, the additive strain decomposition $\boldsymbol{\varepsilon} = \boldsymbol{\varepsilon}^e + \boldsymbol{\varepsilon}^p$ is used, where $\boldsymbol{\varepsilon}$ is the total strain, $\boldsymbol{\varepsilon}^e$ is the elastic strain, and $\boldsymbol{\varepsilon}^p$ is the plastic strain. In the case of large strains, the following multiplicative decomposition of the deformation gradient $\mathbf{J}$ is used. This decomposition is defined as $\mathbf{J} = \mathbf{J}^e\mathbf{J}^p$, where subscripts e and p in this equation refer, respectively, to the elastic and plastic parts. The stress is related to the elastic strain. Since the elastic region, is often relatively small in soils, the linear stress-strain relationship $\boldsymbol{\sigma} = \mathbf{C}^e : \boldsymbol{\varepsilon}^e$ is often sufficient, where $\mathbf{C}^e$ is the fourth order tensor of elastic coefficients, $\boldsymbol{\sigma}$ is the stress tensor, and $\boldsymbol{\varepsilon}^e$ is the elastic strain tensor. While the linear stress-strain relationship has been widely used in many soil models, it is important to point out that some models have incorporated nonlinear elastic relationships in both the small strain (e.g. [19]) and large deformation (e.g. [20]) cases. Such models help correct the amount of elastic strain during large plastic deformation.

The elastic region is defined by a generic yield function $f(\boldsymbol{\sigma}, t)$ shown in Figure 6. When $f < 0$, the stress state is within the elastic region. Plasticity can only occur when $f = 0$, which defines the yield surface. Stress states where $f > 0$ are inadmissible. However, the yield surface may evolve or translate, as discussed below, allowing initially inadmissible stress states after some plastic deformation. The evolution of plastic strain is governed by the flow rule [21,22] $d\boldsymbol{\varepsilon}^p = d\lambda\left(\partial g / \partial \boldsymbol{\sigma}\right)$, where $d\lambda$ is the plastic multiplier, and g is a plastic potential function that determines the direction of plastic flow. If $f = g$, then the flow rule is said to be

associative. Associative flow follows from the principle of maximum plastic dissipation, allowing the body to reach the lowest possible energy state; hence it is commonly employed in the plasticity theory of metals. However, the principle of maximum plastic dissipation tends to overestimate dilatation in soils and other cohesive-frictional materials, and hence many soil models use nonassociative flow rules. While any plasticity model may experience a loss of ellipticity condition that leads to spurious mesh dependency in numerical solutions during softening, nonassociative models may experience loss of ellipticity even during the hardening phase [23], adding a necessity to check for this condition.

The yield function and plastic flow rule together operate under the Kuhn-Tucker optimality conditions $f \leq 0,\ d\lambda \geq 0,\ f \cdot d\lambda = 0$. These conditions appear in many contexts in mathematics and solution techniques are well studied. In incremental form for plasticity, these are typically solved by first assuming that the response is elastic. If the resulting solution violates the first condition, the equation $f = 0$ is then used along with the hardening laws and momentum balance equations to solve for the $\Delta\lambda$ (the finite increment analogue of $d\lambda$) and the other unknown variables.

The last element needed to define a plasticity model is the evolution of internal state variables. The yield surface and plastic potential may not be constant but may evolve with plastic work or strain. For example the size of the yield surface may increase, allowing plastic hardening. The elastic constitutive equation, yield function, flow rule, and hardening laws, together, define the mechanical behavior for a particular model. The equations are usually written in rate form because of the history (path) dependence of the material.

As stated above, the incremental form for plasticity is used to predict the elastic response of the material. This predicted elastic response is known as the trial state. It is typically

found by freezing plastic flow. The trial state is identical to the actual state when the condition $f < 0$ is satisfied. Otherwise the trial solution needs to be corrected for plastic effects; this process is known as return mapping. Loosely speaking, one maps the trial state back to the yield surface so that the condition $f \leq 0$ is always enforced. The mapping can be accomplished using a variety of methods but in most cases the principle of maximum plastic dissipation is used to determine a direction for the correction for plastic flow normal to the yield surface. In certain formulations of the plasticity equations one can use the condition $f = 0$ along with the hardening laws and momentum balance equations to find a closed form solution for $d\lambda$. When this is the case the return mapping can be accomplished in one step and thus is given the name "one-step" return mapping.

While a brief outline of plasticity is provided in this section, a broader overview of plasticity and the constitutive modeling of soils is provided by Scott [24]. Some of the more common soil models are detailed in the following subsections.

3.2 Single Phase Plasticity Models

In this section, single phase homogenized plasticity models are discussed. Here, the soil is treated as a homogenized medium of solid and fluid mass. These models include the Mohr-Coulomb model, the Drucker-Prager and uncapped three-invariant models, modified Cam-Clay and Cap models, and viscoplastic soil models.

Mohr-Coulomb Model The Mohr-Coulomb model is one of the oldest and best-known models for an isotropic soil [25]. Initially the yield surface was used as a failure envelope, and still is in geotechnical practice. It was later adopted as a yield surface for plasticity models. In two dimensions, the yield surface of the Mohr-Coulomb model is defined by a linear relationship between shear stress and normal stress which is written as [26]

$$f = |\tau| - (c - \sigma \tan\phi) = 0 \tag{9}$$

where τ and σ are, respectively, the shear and normal stresses, and the constants c and ϕ are the cohesion and internal friction angle, respectively. In three dimensions, the yield surface is more complicated and is defined by the following equation [26]:

$$f = \frac{1}{3} I_1 \sin\phi + \sqrt{J_2}\sin\left(\theta + \frac{\pi}{3}\right) + \sqrt{\frac{J_2}{3}}\cos\left(\theta + \frac{\pi}{3}\right)\sin\phi - c\cos\phi = 0 \tag{10}$$

where $I_1 = \mathrm{tr}(\boldsymbol{\sigma})$ is the first invariant of the stress tensor $\boldsymbol{\sigma}$, $J_2 = (\boldsymbol{q} : \boldsymbol{q})/2$ is the second invariant of the deviatoric stress tensor $\boldsymbol{q} = \boldsymbol{\sigma} - (1/3) I_1 \mathbf{I}$, and θ is equal to the Lode angle defined by [26]:

$$\cos(3\theta) = \frac{3\sqrt{3}}{2} \frac{J_3}{J_2^{3/2}} \tag{11}$$

where $J_3 = \det(\boldsymbol{q})$ is the third invariant of deviatoric stress tensor and the lode angle θ varies from 0 to 60 degrees. A Mohr-Coulomb yield surface forms a hexagonal pyramid in principal stress space, as shown in Figure 6a. As can be seen from Figure 6a, the yield surface defined by the Mohr-Coulomb model includes discontinuous gradients. These discontinuities add complexity to the return-mapping algorithm. While multi-surface plasticity algorithms have been used to handle this situation, such algorithms are complex and relatively time consuming.

While the Mohr-Coulomb model is still useful in among other things, as a first approximation, most modern vehicle-terrain studies with continuum soil models favor more advanced and sometimes more efficient schemes. An example of an application of the Mohr-Coulomb yield criteria in a tire-snow interaction study can be found in Seta et al. [27]. An explicit finite element method tire model was used in conjunction with a finite volume method approximation of snow using a Mohr-Coulomb yield model. Tire traction tests under differing

tire contact and inflation pressures were conducted. Also, the simulation of the influence of different tread patterns was investigated. It was found that the results agreed well with experimental data.

Drucker-Prager and Uncapped Three-Invariant Models A simpler method to handle the discontinuities apparent in a Mohr-Coulomb model is to use a smooth approximation to the yield surface. Drucker et al. [28] initially proposed a cone in principal stress space (Figure 6b), by adding a pressure-dependent term to the classical von Mises yield surface, resulting in the yield function:

$$f = \sqrt{J_2} + \eta p - \xi c \tag{12}$$

where J_2 and $p = I_1/3$ are invariants of the stress tensor, c is the cohesion, η and ξ are parameters used to approximate the Mohr-Coulomb criterion. Like von Mises plasticity, one-step return-mapping can be achieved for linear hardening, making the model quite efficient to implement. While the associative model over predicts dilatation, nonassociative versions correct this [28]. Initially developed as an elastic-perfectly plastic model (no change in the yield surface on loading), researchers later added hardening of the yield surface parameters to the model in various forms. See, for example, Vermeer and de Borst [29] for a relatively sophisticated phenomenological hardening model.

One of the limitations that this model shares with other plasticity models is that hydrostatic loading and unloading produces considerable hysteresis which cannot be predicted using the same elastic bulk modulus of loading and unloading and a yield surface which does not cross the hydrostatic loading axis for hydrostatic compression [30]. Another limitation being that the cone does not approximate the Mohr-Coulomb hexagonal pyramid well for low friction angles. To account for this last issue, researchers have developed smooth yield surfaces that

better approximated the Mohr-Coulomb yield surface. These yield surfaces have different yield points in triaxial extension versus compression for a given mean stress, like the Mohr-Coulomb yield surface, but are smooth. The Matsuoka and Nakai [31] model actually captures both the extension and compression edges of the Mohr-Coulomb yield surface, unlike the Lade-Duncan model as can be seen from Fig. 7d which has been adapted from [32]. While this fact does not necessarily make the Matsuoka-Nakai yield surface more correct, it does make it easier to fit to standard geotechnical strength tests.

An example of a contemporary simulation of tire-soil interaction using a Drucker-Prager model can be found in Xia [33]. A Drucker-Prager/Cap model which was capable of predicting transient spatial density was implemented in the commercial finite element code ABAQUS. This model was used in representative simulations to provide demonstrations of how the tire/terrain interaction model can be used to predict soil compaction and tire mobility in the field of terramechanics [33]. The model predicted that soil compaction was minimized by increasing the rolling of the simulated tire.

For other examples of tire-terrain studies which include a Drucker-Prager soil the reader is directed to Lee [34], Fassbender et al. [35], or Meschke et al. [36]. The Drucker-Prager model has also been used to capture the behavior of snow, as noted in the referenced articles above. Drucker-Prager models are often used to model snow for their sensitivity to changes to pressure.

The differences in yielding triaxial extension and compression that have been demonstrated in experiments can also be captured by modifying a Drucker-Prager-type yield surface by using a smooth third-invariant modifying function. Two of these functions are developed by Gudehus [37] and William and Warnke [38]. While the former is simpler in form, it is only convex when the ratio of triaxial extension to compression strength, ψ, is greater than

0.69. The William-Warnke function is convex until $\psi = 0.5$. Convexity is essential in yield surfaces to ensure proper return mapping.

A shortcoming of the above models is that they assume a constant ratio between pressure and deviatoric stress, or normal and shear stress, during yielding, that is, a constant friction coefficient; research in soils shows that this is not the case and the friction angle decreases with increasing pressure. Also, modifications to the return mapping algorithm are necessary at the tensile vertex. Furthermore, at high confining pressures, soils may exhibit compactive plasticity due to pore collapse, grain crushing, and other phenomena. With the exception of the compression cap in Xia [33], there are no vehicle-terrain studies which include the above-mentioned modifications or extensions to the Drucker-Prager model.

Modified Cam-Clay and Cap Models The original Cam-Clay model has not been as widely used for numerical predictions of soil response as the modified Cam-Clay (MCC). The qualifier "modified" is often dropped when referring to the modified Cam-Clay model [39]. The modified Cam-Clay model by Roscoe and Burland [40] is based on the critical state theory and was meant to capture the properties of near-normally consolidated clays under triaxial compression test conditions. The yield surface is assumed to have an elliptical relationship between the pressure and magnitude of deviatoric stress that may be expanded with the increase of volumetric strain, as shown in Figure 8. The function for the yield surface of the MCC model is defined as

$$q^2 - M^2\left[p'\left(p'_c - p'\right)\right] = 0 \tag{13}$$

Here, q is the norm of the deviatoric stress, p' is the effective mean stress, the pre-consolidation stress p'_c acts as a internal state parameter, and the stress ratio $M = q/p'$ at critical state is

related to the angle of friction through the relationship $M = 6\sin(\phi)/(3-\sin(\phi))$. The modified Cam-Clay model has been extended to the finite deformation case in Borja and Tamagnini [41].

Cam-Clay models can predict failure and the nonlinear stress-path dependent behaviors prior to failure fairly accurately, especially for clay type soils [30]. This model, however, still has some disadvantages [30]: the behavior near the *p* axis varies from experimental results (Figure 8); points on the yield surface above the critical state line do not satisfy Drucker's postulate of stability; and the shear strain predicted by Cam-Clay models is too high at low stress ratios [42].

An example of a tire-terrain interaction study that includes a Cam-Clay model can be found in Meschke et al. [36]. A finite deformation Cam-Clay model was used to model the mechanical interaction between a tire tread running over a snow covered surface. The material model was calibrated with experimental data of hydrostatic and shear-box tests of snow [36]. The Cam-Clay model was found to realistically replicate an experimentally observed failure mode of snow.

Similarly, a track-terrain study utilizing a Cam-Clay soil model is given in Berli et al. [43]. The compaction sensitivity of a loess soil at different soil moisture conditions was studied. It was found that the observed compaction effects for loess soil were in agreement with the model predictions if the soil was assumed to be partially drained [43]. If the wet subsoil was assumed in fully drained conditions then the predictions disagreed. Also, the moisture dependence of the precompression stress needed to be taken into account in order for the model to agree with the experimental data [43].

There are several advanced derivatives of the Cam-Clay type soil models that include the *three-surface kinematic hardening model* and the *K-hypoplastic model* [44,45]. For instance, the three-surface kinematic hardening (3-SKH) model employs the following kinematic surfaces: the

first surface is defined as the yield surface, the second surface is named the history surface and is the main feature of the 3-SKH model, and the third surface is the state bounding (or boundary) surface. The state boundary surface is sometimes taken to be the MCC surface since it incorporates kinematic hardening [46]. The history surface defines the influence of recent stress history, and the yield surface defines the onset of plastic deformations. Kinematic hardening allows it to better predict load reversals. It has been found that the 3-SKH model can acceptably predict over-consolidated compression behavior for clay but can have difficulty modeling pore pressure variations [44]. The K-Hypoplastic model employs critical state soil mechanics concepts that can be applied to the modeling of fine-grained soils. It can be formulated in two manners; by enhancing the model with the intergranular strain concept, it can be extended to the case of cyclic loading and further improve the model performance in the range of small-strains. Even without the above enhancement, the K-Hypoplastic model is suitable for fine-grained soils under monotonic loading at medium to large strain levels [45]. These derivatives of the MCC model have yet to be included in a vehicle-terrain study.

Cap-plasticity models were developed to address the shortcomings of the Cam-Clay type models. Drucker et al. [47] first proposed that "successive yield surfaces might resemble an extended Drucker-Prager cone with convex end spherical caps" as shown in Figure 7c [48]. As the soil undergoes hardening, both the cone and the end cap expand. This has been the foundation for numerous soil models.

The plastic yield function f in the inviscid cap model of DiMaggio and Sandler [30] is formulated in terms of the first stress invariant I_1 and the second deviatoric stress invariant J_2 [49,50]. As shown in Figure 9, the yield surface is divided into three regions. The cap is a hardening elliptical surface defined as

$$f\left(I_1,\sqrt{J_2},k\right)=\sqrt{J_2}-F_c\left(I_1,k\right)=\sqrt{J_2}-\frac{1}{R}\sqrt{\left[X\left(k\right)-L\left(k\right)\right]^2-\left[I_1-L\left(k\right)\right]^2}=0 \qquad (14)$$

where J_2 is the second invariant of the deviatoric stress $\boldsymbol{q}$, R is a material parameter, and k is a hardening parameter related to the actual plastic volumetric change $\varepsilon_v^p=\mathrm{tr}\left(\boldsymbol{\varepsilon}^p\right)=\varepsilon_{11}^p+\varepsilon_{22}^p+\varepsilon_{33}^p$ through the hardening law $\varepsilon_v^p=W\left(1-\exp^{-DX(k)}\right)$. Where W and D are material parameters and $X(k)$ is the value of I_1 at the end of the cap. In Equation 14, $L(k)$ is the value of I_1 at the intersection of the failure envelope and the cap; $L\left(k\right)=k$ if $k>0$, and $L\left(k\right)=0$ if $k\le 0$. The yield surface is of a Drucker–Prager type modified for nonlinear pressure dependence and is defined by the function

$$f\left(I_1,\sqrt{J_2}\right)=\sqrt{J_2}-F_e\left(I_1\right)=\sqrt{J_2}-\left[\alpha-\gamma\exp\left(-\beta I_1\right)+\theta I_1\right]=0 \qquad (15)$$

where α, β, γ, and θ are material parameters. The tension cutoff surface is defined by $f\left(I_1\right)=I_1-\left(-T\right)$, where T is the tension cutoff value. A number of material parameters are necessary for the elastoplastic cap model: η, N, f_0 in the viscous flow rule to be discussed later; W, D, R, X_0 in the cap surface; α, β, γ, θ in the failure surface; and T in the tension cutoff surface. In addition, the bulk modulus K and the shear modulus G are needed for the elastic soil response. An example of a Cap plasticity model used in a tire-terrain model can be found in Xia [33] which was detailed above.

The *Sandia GeoModel* builds on the Cap model with some modifications. It is capable of capturing a wide variety of linear and nonlinear model features including Mohr-Coulomb and Drucker-Prager plasticity depending on the model parameters incorporated. Unlike the Cap model, the cap surface and shear yield surface are connected in a smooth manner, and the model

also accounts for differences in triaxial extension and compression strength using either Gudehus or William-Warnke modifying function described above. The yield function can be written as

$$f = \left(\Gamma^{\xi}\right)^2 J_2^{\xi} - F_c\left(F_f - N\right)^2 = 0 \tag{16}$$

where Γ^{ξ} accounts for the differences in material strength in triaxial extension and triaxial compression, J_2^{ξ} is the second invariant of the relative stress tensor $\boldsymbol{s}$ - $\boldsymbol{a}$ (here $\boldsymbol{a}$ is a back stress state variable), F_c is a smooth cap modifying function, F_f represents the ultimate limit on the amount of shear the material can support, and N characterizes the maximum allowed translation of the yield surface when kinematic hardening is enabled [19]. The plastic potential function is given by [51]

$$g = \left(\Gamma^{\xi}\right)^2 J_2^{\xi} - F_c^g\left(F_f^g - N\right)^2 \tag{17}$$

where F_c^g and F_f^g play analogous roles in the plastic potential function as their counterparts in the yield function. The Sandia GeoModel suffers from the following limitations: the triaxial extension/compression strength ratio does not vary with pressure and it is computationally intensive when compared to similar idealized models [19]. This model has been further adapted to the Kayenta model [52].

The Sandia GeoModel has yet to be included in tire-terrain interaction studies. However, the kinematic hardening feature captures cyclic loading in interaction cycles, the smooth cap improves efficiency compared to similar cap models, and the flexible nonlinear pressure dependence more accurately captures soil behavior over a range of pressures. Hence, it is a candidate for future studies in vehicle-soil interaction.

Soil is not always an isotropic material. Layering and fracture networks, as well as compaction and other history effects may give the soil higher strength or stiffness in certain

directions. Often the effects impart different strength and stiffness in one plane, and there is a transversely anisotropic version of the Kayenta model. Anisotropy may also be addressed using fabric tensors [53]. Other anisotropic models include the work of Whittle and Kavvadas [54], and the S-CLAY 1 model [55]. Aside from the kinematic hardening mentioned in some of the models, detailed review of anisotropic soil models is beyond the scope of this article, however, and the reader is referred to the above references.

Viscoplastic Soil Models Plasticity models such as those described above do not include strain-rate dependent behavior often observed in soils under rapid loading. These viscous effects are more pronounced in the plastic region of most clay soils and rate independent elastic response is generally adequate for practical engineering applications [56,57]. The models described above can be modified to account for rate-dependent plastic effects. Such viscoplastic models are more accurate under fast loading conditions. However, it is difficult to determine the correct value of the material time parameter (which may not correspond to physical time scale) if the stress history is not known.

Two major types of viscoplastic overlays are the Perzyna and Duvaut-Lions formulations. Perzyna's formulation is among the most widely used viscoplasticity models [58]. In this model, the rate form of the flow rule is used to describe viscous behavior leading to a viscoplastic potential which is identical if not at least proportional to the yield surface [48,50,59]. In *Perzyna's viscoplasticity formulation* [56], the viscoplastic flow rule can be expressed as

$$\dot{\boldsymbol{\varepsilon}}^{vp} = \eta \left\langle \phi(f) \right\rangle \frac{\partial g}{\partial \boldsymbol{\sigma}} \tag{18}$$

where η is a material constant called the *fluidity parameter*, the Macauley bracket $\langle\ \rangle$ is defined as $\langle x \rangle = x + |x|/2$, g is the plastic potential function, and $\phi(f)$ is a dimensionless viscous flow

function commonly expressed in the form $\phi(f) = (f/f_0)^N$, where N is an exponent constant and f_0 is normalizing constant with the same unit as f. The Cap model has been extended to the viscoplastic case using Perzyna's formulations. The viscoplastic cap model is adequate for modeling variety of time dependent behaviors such as high strain rate loading, creep, and stress relaxation [60].

A joint bounding surface plasticity and Perzyna viscoplasticity constitutive model has been developed for the prediction of cyclic and time-dependent behavior of different types of *geosynthetics* [61]. This model can simulate accelerating creep when deviator stresses are close to the shear strength envelope in a q creep test and it can also model the behavior in unloading–reloading and relaxation [62]. It has been noted that for multi-surface plasticity formulations the Perzyna type models have uniqueness issues [63].

Another widely used formulation for viscoplasticity is based on *Duvant-Lions theory* [64]. In this formulation, the viscoplastic solution is constructed through the relevant plastic solution. An advantage of the Duvant-Lions model is that it requires the simple addition of a stress update loop to incorporate it into existing plasticity algorithms. Another advantage is that the viscoplastic solution is guaranteed to deteriorate to the plastic solution under low strain rate [50].

Viscoplasticity is thought to simulate physical material inelasticity behavior more accurately than the plasticity approach. It eliminates potential loss of ellipticity condition associated with elasto-plastic modeling [65]. A viscoplastic GeoModel version, based on the Duvan-Lions framework, was developed with separate viscous parameters for volumetric and shear plasticity. Saliba [66] presents a rate dependent model for tire-terrain analysis as well as a review of the mathematical theory of visco-plasticity.

3.3 Multiphase Models

Soils may either be treated as homogenized continua or as a mixture in which each phase (solid, liquid, and gas) is treated separately. The latter approach is considered to be more accurate, but more complicated to implement. Mixture theory can be used at the continuum level to account for each phase, by tracking the total stress $\boldsymbol{\sigma}$, fluid pore pressure p_w, and a pore air pressure p_a. For saturated soils (no gas phase), an effective stress $\boldsymbol{\sigma}'$ is defined, typically as $\boldsymbol{\sigma} - p_w\mathbf{I}$ (though variations exist). The deformation of the soil skeleton is taken to be a function of the effective stress. Any of the plasticity models above can then be implemented using the effective stress in place of the total stress to determine the solid deformation.

In the unsaturated case, two independent variables are usually used to determine the mechanical response, due to apparent cohesion created by menisci in fluid phase. The total stress may be broken down into a net stress $\boldsymbol{\sigma}''$ for the solid skeleton, and suction stress p_c defined as

$$\boldsymbol{\sigma}'' = \boldsymbol{\sigma} - p_a\mathbf{I}, \quad p_c = p_a - p_w \tag{19}$$

An effective stress and suction may also be used, typically $\boldsymbol{\sigma}' = \boldsymbol{\sigma} - p_a\mathbf{I} + \chi\left(p_a - p_w\right)\mathbf{I}$, where χ is a parameter that varies from 0 for dry soil to 1 for fully saturated. The advantage of this formulation is that it reduces to the standard effective stress at saturation. The solid phase may then be modeled in terms of net stress in suction. Some of the above plasticity and viscoplasticity models have been used, with substantial extensions, to model solid deformation in this framework. In rapid loading, the fluid may be thought of as moving with the solid in the saturated case (undrained), but otherwise fluid flow through the solid matrix needs to be accounted for. In the limit where the fluid has enough time to return to steady state conditions, the material is said to be fully drained. Standard coupled fluid flow-solid deformation finite elements often fail due to volumetric mesh locking phenomena. This shortcoming can be solved

by either using a lower order interpolation scheme for fluid flow equations [67], or by stabilizing the element ([68] and references therein).

The *Barcelona Basic Model* (BBM) proposed by Alonso et al. [69] remains among the fundamental elasto-plastic models for unsaturated soils. The BBM model is an extension of the modified Clam-Clay model that captures many of the mechanical characteristics of mildly or moderately expansive unsaturated soils. As originally proposed by Alonso, utilizing a critical state framework, the BBM is formulated in terms of the hydrostatic pressure $p"$ associated with the net stress tensor $\boldsymbol{\sigma}"$, suction s, and the deviatoric stress $\boldsymbol{q}$. One may write a yield function for the model as follows:

$$f = 3J_2 - \left(\frac{\tilde{g}(\theta)}{\tilde{g}(-30^o)} \right)^2 M^2 \left(p" + (k)(s) \right) \left(P_c - p" \right) \tag{20}$$

where M is the slope of the critical state lines, k is parameter that describes increase in apparent cohesion with suction, P_c is the pre-consolidation pressure, and the function $\tilde{g}(\theta)$ is given by $\tilde{g}(\theta) = \sin\phi' \Big/ \left(\cos\theta + \left(\sin\theta \sin\phi' / \sqrt{3} \right) \right)$, where ϕ' is the friction angle, and θ is the Lode angle. The hardening law is given by the following relationship:

$$dP_0 = \frac{P_0}{\lambda_0^* - \kappa^*} d\,\varepsilon_v^p \tag{21}$$

where P_0 is the hardening parameter defined by the location of the yield surface at zero suction, λ_0^* is the slope modified at the normal compression line, and κ^* is the modified swelling index that is assumed to be independent of suction. The plastic potential is a slight modification of the yield function given by

$$g = 3\alpha J_2 - \left(\left(\frac{g(\theta)}{g(-30^o)} \right)^2 M^2 \left(p" + (k)s \right)\left(P_c - p" \right) \right) \tag{22}$$

where α is defined as $\alpha = M(M-9)(M-3)\left(1/\left(1-k^*/\lambda_o^*\right)\right)/9(6-M)$ [69]. Some of the shortcomings of the BBM model are as follows: the BBM cannot completely describe hydraulic hysteresis associated with wetting and drying paths, it does not give the possible ranges of suction over which shrinkage may occur, and it does not include a nonlinear increase in shear strength with increasing suction.

Elasto-Plastic Cap Model of Partially Saturated Soil This section deals with the extension of a cap model which can describe the material behavior of partially saturated soils, in particular, of partially saturated sands and silts. The soil model is formulated in terms of two stress state variables; net stress $\boldsymbol{\sigma}''$, and matric suction p_c. These stress state variables are defined in Eq. 19.

The yield surface (Figure 10), consisting of a shear failure surface and a hardening cap surface, the plastic potentials for the non-associated flow rule and the hardening law for the cap are extended by taking into account the effects of matric suction on the material behavior. Using net stress and matric suction as stress state variables allows modeling independently the effects of a change in the skeleton stress and of a change in suction effects on the mechanical behavior of the soil skeleton [70]. The functional form of the shear failure surface is

$$f_1\left(\boldsymbol{\sigma}'', p_c\right) = L(\theta)\sqrt{2J_2} - F_e\left(I_1''\right) - F_s\left(p_c\right) \tag{23}$$

where I_1'' denotes the first invariant of the net stress tensor $\boldsymbol{\sigma}''$. In the preceding equation, $L(\theta) = \left(\left(1-\omega\cos 3\theta\right)/\left(1-\omega\right)\right)^{-\eta}$, where ω and η are parameters defining the shape of the yield

surface with respect to the Lode angle θ. In Eq. 23, $F_e\left(I_1''\right)$ defines the shear failure envelope at vanishing matric suction, and $F_s\left(p_c\right)$ accounts for the dependence of the shear strength on the matric suction [70]. These two functions are defined as $F_e\left(I_1''\right)=\alpha+\eta I_1''$ and $F_s\left(p_c\right)=kp_c$, where k is a parameter controlling the increase of the shear failure envelope with increasing matric suction, and α is a material parameter [70]. The functional form of the strain hardening cap is

$$f_2\left(\boldsymbol{\sigma}'',\kappa\left(p_c\right),p_c\right)=F_c\left(\sqrt{2J_2},I_1'',\theta,\kappa\left(p_c\right)\right)-F_e\left(\kappa\left(p_c\right)\right)-F_s\left(p_c\right) \tag{24}$$

with $\kappa\left(p_c\right)\le I_1''\le X\left(\kappa\left(p_c\right)\right)$, and

$$F_c\left(\sqrt{2J_2},I_1'',\theta,\kappa\left(p_c\right)\right)=\sqrt{L^2\left(\theta\right)\left(\sqrt{2J_2}\right)^2+\left(\frac{I_1''-\kappa\left(p_c\right)}{R}\right)^2} \tag{25}$$

The plastic strain rate is determined by the non-associative flow rule $\dot{\boldsymbol{\varepsilon}}^p=\sum_{i=1}^{2}\dot{\gamma}_i\left(\partial g_i/\partial\boldsymbol{\sigma}''\right)$, where $\dot{\gamma}_i$ are the plasticity consistency parameters. The direction of the plastic flow is determined by means of a plastic potential

$$g_1\left(\boldsymbol{\sigma}'',p_c\right)=\sqrt{2J_2}-\alpha-\psi I_1''-F_s\left(p_c\right) \tag{26}$$

In this equation, ψ is a parameter that governs the amount of plastic dilatation. The plastic potential for the strain hardening cap is assumed as

$$g_2\left(\boldsymbol{\sigma}'',\kappa\left(p_c\right),p_c\right)=\sqrt{\left(\sqrt{2J_2}\right)^2+\left(\frac{I_1''-\kappa\left(p_c\right)}{R}\right)^2}-F_e\left(\kappa\left(p_c\right)\right)-F_s\left(p_c\right) \tag{27}$$

The plastic volumetric strain rate is

$$\dot{\varepsilon}_v^p=\lambda\left(p_c\right)\frac{\dot{X}\left(\kappa\left(p_c\right)\right)}{X\left(\kappa\left(p_c\right)\right)} \tag{28}$$

where $X\left(\kappa\left(p_c\right)\right)$ corresponds to the apex of the elliptical cap.

Bounding Surface Plasticity Unsaturated Soil Model Dafalias and Popov [71] developed bounding surface plasticity for metals. This approach was later applied to clays by Dafalias and Herrmann [72], extended to pavement based materials by McVay and Taesiri [73], and to sands by Hashigushi and Ueno [74], Aboim and Roth [75], and Bardet [76]. Bounding surface plasticity provides a framework with which to capture the cyclic behavior of engineering materials. The advantages of this framework over conventional plasticity theory have been investigated for monotonic and cyclic loads. Wong et al. [77] developed a new bounding surface plasticity model, which includes an evolving bounding surface, for unsaturated soils with a small number of parameters based on Bardet's model [76].

The bounding surface plasticity model developed by Wong et al. [77] is elliptical in the plane of effective mean-stress p' and deviatoric stress q with $p' = \left(\sigma_1' + \sigma_2' + \sigma_3'\right)/3$ and using cylindrical symmetry $q = \sigma_1^{'} - \sigma_3^{'}$. The bounding surface can be defined as

$$f\left(\overline{p}', \overline{q}', \varepsilon_p^p, s\right) = \left(\frac{\overline{p}' - A_\pi}{\rho - 1}\right)^2 - \left(\frac{\overline{q}}{M_\pi}\right)^2 - A_\pi^2 \tag{29}$$

where M_π is the slope of the saturated soil critical state line (CSL), $\overline{p}' = \gamma A_\pi$, $\overline{q}' = \gamma x M_\pi A_\pi$, $x = q/\left(Mp' + q_0\right)$, and $\gamma = \left(1 + \left(\rho - 1\right)\sqrt{1 + x^2\rho\left(\rho - 2\right)}\right)\Big/\left(1 + \left(\rho - 1\right)^2 x^2\right)$. M_π and A_π are assumed to be material parameters that are independent of suction *s*. Also, ρ is a material parameter. The bounding surface plasticity soil model has the following limitations and shortcomings [26]: (1) more experimental data is needed to define the suction dependence of material parameters; and (2) an objective relation, defined by the retention curve, is needed between the degree of saturation and suction.

The multiphase models presented above, up to date, have not been included in tire-terrain studies. These models, while more complex, will offer a better approximation for vehicle-terrain interactions than their single phase counterparts.

4. PARTICLE BASED AND MESHFREE METHODS

The finite element method is a widely accepted and used approach to the solution of engineering problems which can be modeled using a continuum approach. However, simulations of explosions, fragmentations, and inherently granular problems require the use of adaptive meshing techniques that can become computationally intensive [78]. Particle-based and meshfree methods offer engineers a new methodology with which they may more accurately tackle highly discrete or granular problems. Particle based methods offer a number of advantages. The connectivity between nodes, or particles, is (re)computed at each time step and this allows for simulations of large deformations [79]. Fracture and other discontinuous behaviors are explicitly captured by particle-based methods. The following is a brief overview of three of the most commonly used particle based and mesh-free methods; the *discrete element method*, *smoothed particle hydrodynamics,* and *reproducing kernel particle methods*.

4.1 Discrete Element Method (DEM)

In the case of the finite element method, the material (soil in this study) is assumed to be a continuum. For the cases in which the granular behavior of soil is to be accurately modeled the discrete element method (DEM) is applied. The DEM was developed to simulate the dynamic behavior of granular material such as granular flow. In the DEM, the material is represented by an assembly of particles with simple shapes (circles and spheres), although there have been simulations in which non-circular rigid particles are used [80,81]. The disadvantages of using

simple shapes, such as spherical grains, are that they are unable to interlock and that they can rotate without dilating the surrounding soil. Poly-ellipsoidal and polyhedral grain shapes may offer a more realistic representation of particulate soil [82], but the contact algorithms are more complicated and solution times can increase significantly.

The elastic and inelastic properties at the contact between the particles are introduced using springs with spring constants (elastic response) and dashpots with viscous damping constants. These model parameters can be difficult to obtain by direct physical measurement. Indirect methods of parameter determination have been developed. Among them, the trial-and-error approach has been used successfully and the method of dimensional analysis combined with biaxial test simulation can obtain best-fit parameters of the DEM model [82].

The contact forces between particles are sometimes calculated from the interpenetration between those particles using the spring constant and the viscous damping constant [83]. The determination of contact between two particles is a computationally intensive component of DEM simulations. For example, if we take the shapes to be ellipsoids and poly-ellipsoids as in Knuth et al. [82], the contact detection algorithm is based on the use of dilated particles. This dilation process is accomplished by placing spheres of a fixed radius on the surface of every particle. One then determines contact between two spheres chosen from the infinite sets of spheres between the two particles [82]. An efficient algorithm is mandatory for such an exhaustive search. Finally, once contact is detected and evaluated, the displacements of the particles are obtained for a certain time interval by solving the governing kinetic equations of motion. This process is repeated for all particles in the analyzed region for very short time intervals until the end of the simulation time.

Some of the shortcomings associated with the discrete element method are as follows: it can be computationally very inefficient for soil in which the granular effect can be approximated using a continuum model [83], it is difficult to accurately determine the spring and damping constants that define the contact forces between the particles [84], and the representation of soil cohesion and adhesion properties is difficult to incorporate within DEM analysis [85]. Nonetheless, there are a number of applications of the discrete element method to tire-soil interaction. As mobility of planetary rovers is of considerable contemporary interest, much work has been done in the simulation of lunar soil-tire interactions; as examples of such work see Nakashima et al. [86] or, as another example, Knuth et al. [82]. An example of such a study can be found in Li et al. [87]. In that study, a discrete element model based on the fractal characteristics, particle shape, and size distribution of returned samples from the Apollo-14 mission was developed. Four basic compound spheres where used to model the lunar particles and the model parameters were found using dimensional analysis. It was found that since subsurface regolith particles are arranged in a looser manner the rover wheel required less drive torque [87].

4.2 Smoothed Particle Hydrodynamics (SPH) and Reproducing Kernel Particle Methods (RKPM)

As one of the earliest meshfree methods, *smoothed particle hydrodynamics* has been widely adopted and used to solve applied mechanics problems. In SPH, the idea is to discretize the material into particles, with each particle having a unique neighborhood over which its properties are "smoothed" by a localized interpolation field, called the kernel function [79]. The neighborhood of each element defines the interaction distance between particles, often referred to as the smoothing length. Smoothed particle hydrodynamics has been used to model soil

behavior. In particular, Bui *et al.* [88] proposed a Drucker-Prager model for elastic-plastic cohesive soils which showed good agreement to experimental results. However, the model suffered from tensile instability which was overcome by using the tension cracking treatment, artificial stress, and other methods.

Other shortcomings associated with SPH methods include: a zero energy mode, difficulty with essential boundary conditions, and an inability to capture rigid body motions correctly. It should be noted that these fundamental issues have been addressed by subsequent SPH formulations [79] but further work is necessary to determine the suitability in tire-terrain applications. Zero energy modes are not only evident in SPH models but they have also been found in finite difference and finite element formulations. SPH suffers from a zero energy mode due to the derivatives of kinematic variables being evaluated (at particle points) by analytical derivatives [79]. The zero energy mode can be avoided by adopting a stress point approach [79]. One of the disadvantages that SPH shares with other particle methods is the difficulty in enforcing essential boundary conditions. The image particle method and the ghost particle approach have been developed to address this issue [79].

SPH interpolants among moving particles cannot represent rigid body motion since SPH is not a partition of unity [79]. This leads to the development of a corrective function; this new interpolant is named the reproducing kernel particle method (RKPM) [79]. RKPM improves the accuracy of the SPH method for finite domain problems [89]. In this method, a modification of the kernel function, through the introduction of a correction function to satisfy reproducing conditions, results in a kernel that reproduces polynomials to a specific order. Unlike traditional SPH methods, the RKPM method can avoid the difficulties resulting from finite domain effects and minimize the amplitude and phase errors through the use of a correction function which

allows for the fulfillment of the completeness requirement. While RKPM methods have not been used in vehicle-terrain interactions, they have been quite successfully applied to geotechnical applications. RKPM methods demonstrate promising potential for large deformation problems but require a systematic approach for the selection of appropriate dilation parameter in order to be made robust [89]. Complexities in meshfree methods, especially with boundary conditions, make them more difficult to couple with other techniques in contact problems.

5. COMPARISON OF SOIL MODELS

The soil models described in Sections 2, 3, and 4 offer a broad overview of the various common methods used in soil modeling. The categories for vehicle-terrain interaction presented in this paper include: empirical, analytical, and semi-empirical, continuum mechanics-based, particle and mesh-free terramechanics methods. Terramechanics studies exist that include a combination of the aforementioned broad categories. Nakashima and Oida [90] present a combined FEA and DEM tire-soil interaction model. Recently, SPH methods have been used in conjunction with FEM to produce tire-soil interaction models [91], but it was concluded that further validation would be required to analyze the effects of SPH parameters on results [92].

5.1 Comparison of Models Based on Soil Characteristics and Geotechnical Applications

Throughout this work, each soil model was presented along with its disadvantages; a brief summary of the advantages of the methods will now be given. Empirical terramechanics models are often invaluable for quick *in situ* trafficability decisions. On the other hand, analytical and semi-empirical terramechanics models are well suited for real time vehicle evaluation for operation in off road environments. In the case of continuum models, the Mohr-Coulomb model

is well known for the simulation of isotropic materials. It is well suited for use as a first approximation in soil modeling. Drucker-Prager models work very well as approximations to materials that exhibit high compressibility. Modified Cam-Clay models work well for clay type materials although they have been applied to the simulations of sand type soils. Viscoplastic formulations are especially suited for scenarios in which the soil is under fast loading conditions. Multiphase models often require the formulation of new finite elements that are capable of capturing the soil skeleton deformation accurately and efficiently. However, these soil mixture approximations are considered a better representation of physical soil. Particle and meshfree models are particularly suited for problems in which the granular aspect of soil plays a prominent role. Along with meshfree methods, they are suited for large deformation problems such as fragmentation and simulation of explosions in soil.

The advantages of each model serve to guide the designer or analyst in the applicability of certain models to a particular problem domain. Plainly stated: model selection depends largely on trade-offs between the behavior of the desired soil being modeled and the availability of material parameter information [93]. At present, there does not exist a soil material model which can capture every soil characteristic in a realistic manner. One must match each model to a particular problem and it is expected that multiple models would be required to fully analyze a complex engineering problem.

Table 1 offers a comparison of the soil models presented in this paper based on the ability of the model to capture work hardening, fracture, cyclic loading, etc. In the table, "CM" implies that if the continuum model has the trait then so does the corresponding model. A comparison between Drucker-Prager and Cam-Clay models has been presented in Chi and Tessier [94]. A similar comparison for snow is published in Meschke et al. [36].

5.2 Comparison Based on Terramechanics Applications

Comparisons can be made between the broad categories of soil models. Early empirical terramechanics models were not formulated in terms of design parameters used to evaluate the effectiveness of vehicles in varying terrains. This has been a major disadvantage of their use. The semi-empirical terramechanics approach remains among the most popular methods used for vehicle-terrain interaction studies in MBS simulations [95]. This popularity can be attributed to the efficiency of most implementations for analytical terramechanics. However, Azimi et al. [96] has concluded that the Bekker and Wong models need further improvement and validation. The dynamic terramechanics models presented above offer a good starting point for such improvements. Of the FEA, particle based, and mesh-free methods, the DEM is unattractive due to its computational cost and inherent difficulty in capturing cohesive and adhesive tensile phenomena of soil (though it can capture soil rupture and other particle phenomenon quite easily). Mesh-free methods are computationally intensive and require further testing and validation [92]. While FEA and DEM methods are gaining popularity, the initial resistance towards the use of these methods was due to the computational intensity required for such vehicle-terrain interaction. Considerable progress in computational power of personal computing systems is making this avenue of analysis more appealing. FEA implementations of soil plasticity that employ highly efficient algorithms have been developed in recent decades, often with quadratic rates of convergence, for the solution of the plasticity equations. Leveraging these algorithms within a FEA/MBS environment will allow for the development of high fidelity vehicle-terrain interaction models.

Over the last decade or so there have been a number of studies which have presented the results of modeling the interaction between rigid and deformable tires on soft terrain simulated

using the continuum terramechanics approach. The results of a literature review of continuum based terramechanics studies are presented in Table 2. For a summary of such interaction studies prior to the year 2000, see Shoop [93] or Liu and Wong [97]. From the table we see that there is a clear trend towards the conduction of such interaction studies the closer we move to our present time. Also, all of the reviewed tire-continuum soil interaction studies were found to be undertaken within a FE framework.

As can be seen from Table 2, almost all of the terramechanics applications with continuum soil models investigate the interaction between tire and soft soil. However, in [98], Grujicic et al. investigated the interaction of a standard and up-armored full vehicle on soft soil under several off-road maneuvers. For the study, the soft soil was modeled using the parametric CU-ARL sand model. The vehicle consisted of interconnected subcomponents which include the chassis, suspension system, and multilayered tire modeled using a combination of structural finite elements. It was found that the up-armoring of the vehicle negatively impacted the stopping distance and traction in a straight-line flat-land braking scenario. In a straight-line off-angle downhill braking scenario it was found that up-armoring caused increase vehicle instability and a propensity for the vehicle to roll over. Similar or higher fidelity simulations offer an attractive method for vehicle design and evaluation.

Xia and Yang [99] provide a four tire - soft soil simulation in which they studied the dynamic tire - soft soil interaction in a straight-line scenario. A suspension - less set of four tires was used to investigate soil compaction and rutting and it was found that the transient spatial density due to compaction with geometric nonlinearity can be directly predicted. It is important to note the study was not meant to investigate the tractive phenomenon between tire and soft soil and so the use of a tread-less tire was justified; this was also the case in Shoop [93]. The contact

patch and stress distribution of the tires was investigated and it was found that the tire contact areas are not constant. Also, they are neither rectangular nor circular and so the conventional assumptions of certain other terramechanics approaches are not accurate.

The two studies summarized above represent the vehicle - soft terrain interaction studies conducted in the past decade. While the literature may be weak for vehicle - terrain interaction studies using a continuum mechanics approach, there exists a number of tire - soft soil interaction studies that can serve as a foundation for developing more detailed vehicle - terrain models. The reader is encouraged to consult the references given in Table 2 for details on the topics discussed below.

Almost all of the tire - soft soil models investigated in this review offered a simulation of the tire contact stress distribution and the contact area. It is one of the advantages of using a FEA approach to terramechanics that the dynamic variation in the contact area can be realistically modeled.

Hambleton and Drescher [100] investigated the differences between modeling the tire - soft soil interaction as a two-dimensional and three-dimensional process. It was found that the rolling resistance of a tire modeled as a two and three-dimensional processes agree qualitatively but wheel penetration and material deformation are considerably different, especially for narrow wheels. Nankali et al. [101] studied the response of soil under vertical loading conditions with a multilayered tire model. Their study focused on the effects of tire inflation on stress prediction in the tire and soil, which was found to be modeled sufficiently as a two-dimensional process.

It is known that interfacial behavior related to frictional response is very important in soil compaction and traction simulation [99]. Shoop [93], Liu and Wong [97] discuss the suitability of the coulomb friction law often used in simulations in conjunction with penalty and kinematic

contact methods. They find that a modified law is necessary to more accurately define the traction characteristics of tire - soft soil interaction. While many of the studies surveyed use both coulomb friction law together with a penalty contact method, further work is needed in determining a better model for the frictional response between deformable tire and soft terrain.

One may use a rigid wheel assumption for light loads on soft soil, however, for general simulation needs one should take into consideration the flexible nature of the tire [102]. The material models used to simulate tire behavior range from linear elastic [103] to various hyperelastic formulations (see for example [104]). It is it generally accepted that nearly incompressible hyperelastic formulations more closely model the behavior of rubber tires. Also, it has been found that in order to best describe the deformable behavior of the tires, multilayered tire models are necessary. A unique approach used to accomplish this can be found in Shoop [93]. In that study the combined effects of the layers of the tire are taken into consideration by using a modal analysis approach. Similarly, in order to best describe the traction and interfacial behavior of such models, consideration of the detailed tire tread is necessary.

In order to reduce the computational load required for simulation, it may be advantageous to model the soil using multiple layers (with varying properties) and variable mesh coarseness. As can be seen from the table, the multiple soil layer approach has not been as widely adopted. Xia [33] adopted a multi-layered soil approach and was able to efficiently model the spatial density change in soil. It is hoped that future investigations will take advantage of using multi-layered soils to reduce the computational demand of high-fidelity models.

One last consideration that can be gleaned from Table 2 is that with the exception of a few investigations, almost all of the tire - soft soil investigations that employ a continuum soil model employ a modified Drucker-Prager/Cap plasticity model. Considering that one soil model

cannot capture all necessary phenomenon, it is hoped that future investigations will venture to adopt alternate soil models so that comparisons with regards to terramechanics related issues can be made in earnest between the soil models.

Considering the continuum-based soil models category of Table 1, it can be seen that of the soil plasticity models presented not many capture work hardening, nonlinear pressure dependence, and cyclic loading. Cam-Clay type soil models offer an attractive entry to the modeling of soils through FEA plasticity theory because of the sequential developments of these types of models and the general acceptance of such models in the geomechanics community. Cam-Clay models began with infinitesimal strain assumptions and have been developed to the case of finite strains. Furthermore, Cam-Clay models have been extended to capture the cyclic behavior of soils [105]. While Cam-Clay models remain among the most popular constitutive approximations of soil, they suffer from convergence issues [93]. This should be kept in mind when working with such models.

6. INTEGRATION OF SOIL PLASTICITY WITH ANCF/MBS ALGORITHMS

As previously mentioned, all MBS commercial computer codes do not have the capability of modeling continuum-based soils. Many MBS codes are not designed for large deformations and do not allow for the use of general constitutive equations when structural finite elements are used. This paper aims at addressing this deficiency as part of its objective and critical analysis. The FE implementation of the soil mechanics plasticity equations requires the use of an approach that allows employing general constitutive models. The vehicle/soil interaction can lead to a significant change in geometry that cannot be captured using finite elements that employ only translational displacement coordinates without significant refinement. In some soil applications,

such a significant change in geometry may require the use of elements that employ gradients and accurately capture curvature changes. This requirement can be met using the FE *absolute nodal coordinate formulation* (ANCF) [106]. In this and the following section, the integration of ANCF/MBS and continuum-based soil models is discussed. The finite deformation Cam-Clay soil model proposed by Borja and Tamagnini [41] is used as an example.

6.1 Absolute Nodal Coordinate Formulation (ANCF)

Because of the challenges in integrating the vehicle and environment models, most of the investigations that employ continuum-based environment models in vehicle dynamics are based on a co-simulation approach that requires the use of two different computer codes: an FE code and a MBS dynamics codes. The MBS code is used for solving the system differential/algebraic equations, while the FE code is used for the large deformation analysis and prediction of forces and state variables that are made available to the MBS code. This co-simulation approach is also used to develop FE tire models. The co-simulation approach allows only for exchanging state variables and forces between the two codes; but does not allow for a unified treatment of the algebraic constraint equations that must be satisfied at the position, velocity, and acceleration levels in the MBS algorithms. This paper proposes a method that can be considered as a departure from the co-simulation approach.

ANCF finite elements, which can be used for both tires and soils and can be integrated with MBS algorithms, do not employ infinitesimal or finite rotations as nodal coordinates; instead, absolute slopes and displacements at the nodal points are used as the element nodal coordinates. The position vector $\mathbf{r}^j$ of an arbitrary point on element j can be defined in a global coordinate system XYZ as $\mathbf{r}^j = \mathbf{S}^j\left(x^j, y^j, z^j\right)\mathbf{e}^j\left(t\right)$. In this equation, x^j, y^j, and z^j are the

element spatial coordinates, $\mathbf{S}^j$ is the shape function matrix, $\mathbf{e}^j$ is the vector of element nodal coordinates, and t is time. The nodal coordinate vector $\mathbf{e}^{jk}$ at node *k* can be defined as follows:

$$\mathbf{e}^{jk} = \left[\mathbf{r}^{jkT} \quad \left(\frac{\partial \mathbf{r}^{jk}}{\partial x^j} \right)^T \quad \left(\frac{\partial \mathbf{r}^{jk}}{\partial y^j} \right)^T \quad \left(\frac{\partial \mathbf{r}^{jk}}{\partial z^j} \right)^T \right]^{\mathrm{T}} \tag{30}$$

While fully parameterized ANCF finite elements do not exclude the use of any elastic force formulation, they allow using a general continuum mechanics approach to define the Green-Lagrange strain tensor $\boldsymbol{\varepsilon} = \left(\mathbf{J}^T \mathbf{J} - \mathbf{I} \right) / 2$, where $\mathbf{J}$ is the matrix of position vector gradients. This matrix of position vector gradients can also be used to evaluate the right and left Cauchy-Green deformation tensors whose invariants enter in the formulation of several popular continuum-based soil models that include the Cam-Clay soil models previously discussed in this paper. Using the ANCF description, the left Cauchy-Green deformation tensor $\mathbf{C}_l$ can be evaluated in terms of the ANCF coordinates as $\mathbf{C}_l = \mathbf{J}\mathbf{J}^T$, where the matrix of position vector gradients $\mathbf{J}$ can be expressed in terms of the ANCF gradients at an arbitrary point on the soil. In large strain plasticity formulations, the multiplicative decomposition $\mathbf{J} = \mathbf{J}^e \mathbf{J}^p$ is used, where $\mathbf{J}^e$ is associated with the elastic deformation, and $\mathbf{J}^p$ is associated with the plastic deformation. In a similar manner, the left Cauchy-Green deformation tensor can be decomposed multiplicatively as $\mathbf{C}_l = \mathbf{C}_l^e \mathbf{C}_l^p$, where superscripts *e* and *p* refer, respectively, to elastic and plastic. In the Cam-Clay model discussed in the preceding section, the soil constitutive equations are formulated in terms of the logarithms of the invariants of the elastic Cauchy-Green deformation tensor $\mathbf{C}_l^e$. It can be shown that $\mathbf{C}_l^e$ can be written as $\mathbf{C}_l^e = \mathbf{J}^e \mathbf{J}^{eT} = \mathbf{J} \left(\mathbf{C}_l^p \right)^{-1} \mathbf{J}^T$. ANCF fully parameterized plate and solid finite elements ensure continuity of the gradients at the nodal points and can capture the change in the soil geometry as the result of its interaction with the vehicle. These

elements allow for systematically evaluating the matrix of position vector gradients **J** and the left and the elastic left Cauchy-Green deformation tensors $\mathbf{C}_l$ and $\mathbf{C}_l^e$. The evaluation of these three tensors requires the use of full parameterization. In the Cam-Clay model discussed in the preceding section, the elastic strain measures used are $\varepsilon_i^e = \ln\left(\lambda_i^e\right), i = 1,2,3$, where $\left(\lambda_i^e\right)^2$ is the *i*th principal value of the elastic left Cauchy-Green deformation tensor $\mathbf{C}_l^e$ [41]. One can then define the deviatoric strain vector $\mathbf{e}^e = \boldsymbol{\varepsilon}^e - (1/3)\varepsilon_v^e \boldsymbol{\delta}$, with $\varepsilon_v^e = \boldsymbol{\varepsilon}^e \cdot \boldsymbol{\delta}$ as the volumetric strain invariant. One can also define a deviatoric strain invariant as $\varepsilon_s^e = \sqrt{2/3}\left\|\mathbf{e}^e\right\|$. If $\varepsilon_i^e, i = 1,2,3$ can be determined from the solution of the plasticity equations, the principal values λ_i^e can be determined. It can be shown that in isotropic plasticity models such as this one that the trial principal directions are the same as the current principal directions. Hence the deformation tensor $\mathbf{C}_l^e$ can be determined. In the Cam-Clay model, the principal directions of the effective Cauchy stress tensor $\boldsymbol{\sigma}_K$ are assumed to coincide with the principal directions of the elastic left Cauchy-Green deformation tensor $\mathbf{C}_l^e$.

ANCF representations can also be used to develop accurate geometry of complex-shaped terrains as well as tires and track links. This is another important ANCF feature that distinguishes this new formulation from other existing FE formulations which are not compatible with computational geometry methods. B-spline and NURBS (**N**on-**U**niform **R**ational **B**-**S**plines) cannot in general be converted to other FE formulation meshes without geometry distortion. On the contrary, B-spline and NURBS representations can be converted to ANCF meshes using a linear transformation that preserves the geometry; thereby ensuring that the geometry and the analysis models are the same.

In dynamic soil, tire, and track problems, ANCF leads to a constant inertia matrix and to zero Coriolis and centrifugal forces. The mass matrix obtained using ANCF finite elements can always be written as $\mathbf{M}^j = \int_{V^j} \rho^j \mathbf{S}^{jT} \mathbf{S}^j dV^j$, where ρ^j and V^j are, respectively, the mass density and reference volume of the finite element. While the inertia may not be important in some soil applications, it is important in the case of spinning tires and rotating track links. In fact, new meshes with constant inertia and linear connectivity conditions can be developed for tracked vehicles using ANCF finite elements. These new ANCF finite element meshes can be used to significantly reduce the number of nonlinear algebraic constraint equations of the joints and achieve an optimum sparse matrix structure, as will be explained in Section 7.

6.2 Dynamic Equations

For a finite element or a deformable body, the principle of virtual work can be written using the reference configuration as

$$\int_V \rho \ddot{\mathbf{r}}^T \delta \mathbf{r} dV + \int_V \boldsymbol{\sigma}_{P2} : \delta \boldsymbol{\varepsilon} dV - \int_V \mathbf{f}_b^T \delta \mathbf{r} dV = 0 \tag{31}$$

In this equation, V is the reference volume, ρ is the mass density, $\mathbf{r}$ is the global position vector of an arbitrary point, $\boldsymbol{\sigma}_{P2}$ is the second Piola Kirchhoff stress tensor, $\boldsymbol{\varepsilon}$ is the Green-Lagrange strain tensor, and $\mathbf{f}_b$ is the vector of body forces. The second term in the preceding equation can be recognized as the virtual work of the internal forces, it can be rewritten to define the generalized internal forces, that is

$$\delta W_s = \int_V \boldsymbol{\sigma}_{P2} : \delta \boldsymbol{\varepsilon} dV = \mathbf{Q}_s^T \delta \mathbf{e} \tag{32}$$

where $\delta \mathbf{e}$ is the virtual change in the nodal coordinates associated with a particular ANCF finite element or a body, and $\mathbf{Q}_s$ is the vector of the generalized internal forces. The vector of internal

forces often takes a fairly complicated form, especially in the case of plasticity formulations, and is obtained using numerical integration methods. Equation 32 allows for systematically incorporating the continuum mechanics based soil models discussed in this paper. It also allows for the systematic implementation of the return mapping algorithm required for the solution of the soil plasticity problem as will be explained in Section 7 of this paper. The principle of virtual work leads to the following equations of motion:

$$\mathbf{M}\ddot{\mathbf{e}} + \mathbf{Q}_{\mathbf{s}} - \mathbf{Q}_{\mathbf{e}} = \mathbf{0} \tag{33}$$

where $\mathbf{M}$ is the constant symmetric mass matrix, and $\mathbf{Q}_e$ is the vector of body applied nodal forces.

As previously mentioned, the plasticity equations of the Cam-Clay model are formulated in terms of the logarithms of the invariants of the left Cauchy-Green deformation tensor $\mathbf{C}_l^e$ and the invariants of the Kirchhoff stress tensor $\boldsymbol{\sigma}_K$. These invariants are used in the formulation of the yield function, the flow rule, the hardening law, etc. The ANCF implementation allows for systematically developing the elastic/plastic force of such a Cam-Clay model in a straight forward manner using both fully parameterized ANCF plate and solid elements. In the finite deformation Cam-Clay model discussed in this investigation as an implementation example, the yield function f is expressed in terms of two invariants, the mean normal and deviatoric effective Kirchhoff stress invariants P and Q as $f = \left(Q/M\right)^2 + P\left(P - P_c\right)$, where M is a material parameter that defines the aspect ratio of the Cam-Clay ellipsoid, P_c is a effective Kirchhoff plastic variable (pre-consolidation pressure parameter), $P = \left(1/3\right)\boldsymbol{\beta}.\boldsymbol{\delta}$, and $Q = \sqrt{3/2}\left\|\mathbf{s}\right\|$ with $\boldsymbol{\beta} = \begin{bmatrix}\beta_1 & \beta_2 & \beta_3\end{bmatrix}^T$ is the set of the principal values of the Kirchhoff stress

tensor, $\boldsymbol{\delta} = \begin{bmatrix} 1 & 1 & 1 \end{bmatrix}^T$, and $\mathbf{s} = \boldsymbol{\beta} - P\boldsymbol{\delta}$ [41]. The stored energy function ψ that defines the constitutive relations is expressed in terms of two strain invariants ε_v^e and ε_s^e, previously defined in this section. Using these two invariants, the stored energy function ψ can be defined as $\psi\left(\varepsilon_v^e, \varepsilon_s^e\right) = -P_0\hat{\kappa}e^{\Omega} + (3/2)\mu^e\varepsilon_s^{e2}$, where μ^e is the shear modulus, $\hat{\kappa}$ is the elastic compressibility, $\Omega = \left(\varepsilon_v^e - \varepsilon_{v0}^e\right)/\hat{\kappa}$, and ε_{v0}^e is the volumetric strain at a reference stress. Using the stored energy function, the constitutive equations of the model are defined as $\boldsymbol{\beta} = \left(\partial\psi/\partial\boldsymbol{\varepsilon}^e\right) = \left(\partial\psi/\partial\varepsilon_v^e\right)\left(\partial\varepsilon_v^e/\partial\boldsymbol{\varepsilon}^e\right) + \left(\partial\psi/\partial\varepsilon_s^e\right)\left(\partial\varepsilon_s^e/\partial\boldsymbol{\varepsilon}^e\right)$, where $\partial\varepsilon_v^e/\partial\boldsymbol{\varepsilon}^e = \boldsymbol{\delta}$, $\varepsilon_s^e/\partial\boldsymbol{\varepsilon}^e = \sqrt{2/3}\hat{\mathbf{n}}$, and $\hat{\mathbf{n}} = \mathbf{e}^e/\left\|\mathbf{e}^e\right\|$. It follows that

$$\boldsymbol{\beta} = \partial\psi/\partial\boldsymbol{\varepsilon}^e = P\boldsymbol{\delta} + \sqrt{2/3}Q\hat{\mathbf{n}} = P\boldsymbol{\delta} + \mathbf{s} \tag{34}$$

where

$$P = \left(\partial\psi/\partial\varepsilon_v^e\right) = P_0 e^{\Omega\left(1+\frac{3\alpha\left(\varepsilon_s^e\right)^2}{2\hat{\kappa}}\right)}, \quad Q = \partial\psi/\partial\varepsilon_s^e = 3\left(\mu_0 - \alpha P_0 e^{\Omega}\right)\varepsilon_s^e \tag{35}$$

In this model, the elastic shear modelus is defined as $\mu^e = \mu_0 + \left(\alpha\tilde{\psi}/\hat{\kappa}\right)$ where α is a constant coefficient, and $\tilde{\psi} = -P_0\hat{\kappa}e^{\Omega}$.

The Cam-Clay model proposed by Borja and Tamagnini [41] leads to a constitutive model that has certain features that can be exploited in the design of the solution algorithm. The isotropic property, which is assumed in this model, makes the principal directions of Cauchy stress tensor $\boldsymbol{\sigma}_K$ the same as the principal directions of the elastic left Cauchy-Green deformation tensor $\mathbf{C}_l^e$. In this model, the stored energy function ψ is assumed to depend on $\mathbf{C}_l^e$. The Cauchy stress tensor is defined as $\boldsymbol{\sigma}_K = 2\left(\partial\psi/\partial\mathbf{C}_l^e\right)\mathbf{C}_l^e$. Because of the isotropy property of this

model, one has $\left(\partial\psi/\partial\mathbf{C}_l^e\right)\mathbf{C}_l^e = \mathbf{C}_l^e\left(\partial\psi/\partial\mathbf{C}_l^e\right)$. One can use this identity to show that $\boldsymbol{\sigma}_K$ and $\mathbf{C}_l^e$ have the same principal directions. To this end, we write the eigenvalue problem $\left(\left(\partial\psi/\partial\mathbf{C}_l^e\right)\mathbf{C}_l^e\right)\mathbf{n} = (\beta/2)\mathbf{n}$, where $\mathbf{n}$ is the principal direction of $\boldsymbol{\sigma}_K$. One can also write $\left(\mathbf{C}_l^e\left(\partial\psi/\partial\mathbf{C}_l^e\right)\right)\mathbf{n} = \mathbf{C}_l^e\left(\left(\partial\psi/\partial\mathbf{C}_l^e\right)\mathbf{n}\right) = (\beta/2)\mathbf{n}$. Multiplying both side of this equation by $\left(\partial\psi/\partial\mathbf{C}_l^e\right)$, one obtains $\left(\partial\psi/\partial\mathbf{C}_l^e\right)\mathbf{C}_l^e\left(\left(\partial\psi/\partial\mathbf{C}_l^e\right)\mathbf{n}\right) = (\beta/2)\left(\left(\partial\psi/\partial\mathbf{C}_l^e\right)\mathbf{n}\right)$. This equation shows both vectors $\left(\partial\psi/\partial\mathbf{C}_l^e\right)\mathbf{n}$ and $\mathbf{n}$ have the same direction. It follows that $\mathbf{C}_l^e\left(\left(\partial\psi/\partial\mathbf{C}_l^e\right)\mathbf{n}\right) = \mathbf{C}_l^e(\chi\mathbf{n}) = (\beta/2)\mathbf{n}$, where χ is a scalar multiplier. This latter equation shows that $\mathbf{n}$ is also a principal direction of $\mathbf{C}_l^e$.

The Cam-Clay model analysis presented in this section shows that if ε_v^e and ε_s^e are known, one can determine the mean normal and deviatoric effective Kirchhoff stress invariants P and Q of Eq. 34. If $\hat{\mathbf{n}}$ is known, then the principal values of effective Kirchhoff stress tensor $\beta_i, i = 1,2,3$, can be determined using Eq. 34. Using the principal values $\beta_i, i = 1,2,3$, the Kirchhoff stress tensor $\boldsymbol{\sigma}_K$ can be calculated if the principal directions $\mathbf{n}_i, i = 1,2,3$ of this tensor are known. The second Piola-Kirchhoff stress tensor can then be determined as $\boldsymbol{\sigma}_{P2} = \mathbf{J}^{-1}\boldsymbol{\sigma}_K\mathbf{J}^{-1T}$. This tensor can then be used with the Green-Lagrange strain tensor to formulate the ANCF force vector $\mathbf{Q}_s$ of Eq. 32. The procedure for determining ε_v^e, ε_s^e, β_i, $\hat{\mathbf{n}}$, and $\mathbf{n}_i$ will be discussed in the following section.

7. INTEGRATION WITH MBS ALGORITHMS

In addition to identifying a weakness in the literature in the area of continuum-based soil/vehicle interaction, one of the objectives of this paper is to propose an approach that can be considered as a departure from the co-simulation approach used in the large deformation analysis of MBS applications. In the co-simulation approach, two independent computer codes are used. The first is a MBS code that allows for solving the differential and algebraic equations, while the second is an FE code that allows for the analysis of large deformations. By adopting ANCF finite elements, the use of the co-simulation approach is not necessary since ANCF finite elements can be used to develop a unified framework for the treatment of the constraints and the analysis of large deformations. The goal is to be able to develop new computational environment that allow for the simulations of the interaction of soil and complex MBS vehicles as the one shown in Figure 11.

The main objective of this paper, however, is to present a review of soil mechanics formulations that can be integrated with computational MBS algorithms used for the virtual prototyping of vehicle systems. These algorithms allow for modeling rigid, flexible, and very flexible bodies. The small deformation of flexible bodies in vehicle systems are often examined using the *floating frame of reference* (FFR) formulation. Therefore, efficient modeling of complex vehicle system dynamics requires the implementation of different formulations that can be used for rigid body, small deformation, and large and plastic deformation analyses. A Newton-Euler or Lagrangian formulation can be used to model rigid bodies, the FFR formulation that employs two sets of coordinates (reference and elastic) can be used to model small deformations, and ANCF finite elements can be used to model large and plastic deformations including soil deformations.

7.1 Integration of FE/MBS Algorithms

MBS algorithms are designed to exploit the sparse matrix structure of the resulting dynamic equations. Because ANCF finite elements lead to a constant inertia matrix, Cholesky coordinates can be used to obtain an identity generalized mass matrix, leading to an optimum sparse matrix structure. Computational MBS algorithms are also designed to solve a system of differential and algebraic equations. The differential equations define the system equations of motion, while the algebraic equations define the joint constraints and specified motion trajectories. The nonlinear algebraic constraint equations can be written in a vector form as $\mathbf{C}(\mathbf{q},t)=\mathbf{0}$, where $\mathbf{q}$ is the vector of the system generalized coordinates, and t is time. Using the constraint equations and the equations of motion, the augmented form of the equations of motion can be written as [107]:

$$\begin{bmatrix} \mathbf{M}_{rr} & \mathbf{M}_{rf} & \mathbf{0} & \mathbf{C}_{\mathbf{q}_r}^{\mathrm{T}} \\ \mathbf{M}_{fr} & \mathbf{M}_{ff} & \mathbf{0} & \mathbf{C}_{\mathbf{q}_f}^{\mathrm{T}} \\ \mathbf{0} & \mathbf{0} & \mathbf{M}_{aa} & \mathbf{C}_{\mathbf{q}_a}^{\mathrm{T}} \\ \mathbf{C}_{\mathbf{q}_r} & \mathbf{C}_{\mathbf{q}_f} & \mathbf{C}_{\mathbf{q}_a} & \mathbf{0} \end{bmatrix} \begin{bmatrix} \ddot{\mathbf{q}}_r \\ \ddot{\mathbf{q}}_f \\ \ddot{\mathbf{q}}_a \\ \boldsymbol{\lambda} \end{bmatrix} = \begin{bmatrix} \mathbf{Q}_r \\ \mathbf{Q}_f \\ \mathbf{Q}_a \\ \mathbf{Q}_c \end{bmatrix} \tag{36}$$

where subscripts r, f and a refer, respectively, to reference, elastic, and absolute nodal coordinates, $\mathbf{M}_{rr}$, $\mathbf{M}_{rf}$, $\mathbf{M}_{fr}$, $\mathbf{M}_{ff}$ are the inertia sub-matrices that appear in the FFR formulation, $\mathbf{M}_{aa}$ is the ANCF constant symmetric mass matrix, $\mathbf{C}_{\mathbf{q}}$ is the constraint Jacobian matrix, $\boldsymbol{\lambda}$ is the vector of Lagrange multipliers, $\mathbf{Q}_r$, $\mathbf{Q}_f$, and $\mathbf{Q}_a$ are the generalized forces associated with the reference, elastic, and absolute nodal coordinates, respectively, and $\mathbf{Q}_c$ is a quadratic velocity vector that results from the differentiation of the kinematic constraint equations twice with respect to time, that is $\mathbf{C}_{\mathbf{q}}\ddot{\mathbf{q}}=\mathbf{Q}_c$. The generalized coordinates $\mathbf{q}_r$ and $\mathbf{q}_f$ are used in the FFR formulation to describe the motion of rigid and flexible bodies that experience small deformations. The vector $\mathbf{q}_a$ is the vector of absolute nodal coordinates used to

describe the motion of flexible bodies that may undergo large displacement as well as large and plastic deformations as in the case of soils. The vector $\mathbf{q}_a$ includes the ANCF coordinates, which can be the nodal coordinates $\mathbf{e}$ of all ANCF bodies including the ANCF soil coordinates or the ANCF Cholesky coordinates. Similarly, the mass matrix $\mathbf{M}_{aa}$ includes the soil inertia matrix as well as the inertia of the vehicle components modeled using ANCF finite elements. This mass matrix can be made into an identity mass matrix using Cholesky coordinates, leading to an optimum sparse matrix structure. Using the Cholesky transformation $\mathbf{B}_c$, the nodal coordinates $\mathbf{e}$ can be expressed in terms of the Cholesky coordinates $\mathbf{p}$ as $\mathbf{e} = \mathbf{B}_c\mathbf{p}$. Using this Cholesky transformation, the mass matrix $\mathbf{M}_{aa}$ reduces to an identity mass matrix [108]. The generalized force vector $\mathbf{Q}_a$ includes also the contributions of the forces $\mathbf{Q}_e$ and $\mathbf{Q}_s$ of Eq. 33. The vectors $\mathbf{Q}_e$ and $\mathbf{Q}_s$ account for the vehicle soil interaction forces.

The solution of Eq. 36 defines the vector of accelerations and Lagrange multipliers. The independent accelerations can be integrated to determine the coordinates and velocities including those of the soil. The soil coordinates can be used to determine the total strain components that enter into the formulation of the soil constitutive equations. Knowing the strains, the soil properties, yield function, and the flow rule; the state of soil deformation (elastic or plastic) can be determined as previously discussed in this paper. Knowing the state of deformation, the constitutive model appropriate for this state can be used to determine the elastic force vector $\mathbf{Q}_s$. Therefore, the structure of Eq. 36 allows for systematically integrating soil models into MBS algorithms used in the virtual prototyping of complex vehicle systems. The Cam-Clay soil model proposed by Borja and Tamagnini [41] is considered as an example to explain how the solution of the FE/MBS equations can be used to solve the soil plasticity problem. Efficient

solution of the plasticity equations requires the use of the *return mapping algorithm*. In order to use this algorithm, the soil plasticity equations in their rate form are converted to a system of nonlinear algebraic equations using one of the existing integration formulas.

7.2 Solution of the Soil Plasticity Equations

As explained in the preceding section, in the Cam-Clay model proposed by Borja and Tamagnini [41], one needs to determine ε_v^e and ε_s^e , which can be used to determine the mean normal and deviatoric effective Kirchhoff stress invariants P and Q of Eq. 34. If $\hat{\mathbf{n}}$ is known, one can use Eq. 34 to determine the principal values of Kirchhoff stress tensor $\beta_i, i=1,2,3$, which can be used to determine the Kirchhoff stress tensor $\boldsymbol{\sigma}_K$, provided that the principal directions $\mathbf{n}_i, i=1,2,3$ of this tensor are known. The second Piola-Kirchhoff stress tensor $\boldsymbol{\sigma}_{P2}=\mathbf{J}^{-1}\boldsymbol{\sigma}_K\mathbf{J}^{-1T}$ can be determined and used with the Green-Lagrange strain tensor to formulate the ANCF force vector $\mathbf{Q}_s$ of Eq. 32. In this section, the procedure for determining ε_v^e, ε_s^e, $\beta_i, i=1,2,3$, $\hat{\mathbf{n}}$, and $\mathbf{n}_i, i=1,2,3$ will be discussed.

Using the ANCF coordinates at the current time step, the matrix of position vector gradients $\mathbf{J}$ can be evaluated. In order to solve the Cam-Clay plasticity equations, one defines the trial elastic left Cauchy-Green Lagrange deformation tensor $\left(\mathbf{C}_l^e\right)^{tr}=\mathbf{J}\left(\mathbf{C}_l^e\right)_n\mathbf{J}^T$, where subscript *n* refers to previous time step. Clearly, using ANCF coordinates at the current time step, one can evaluate $\left(\mathbf{C}_l^e\right)^{tr}$ In the Cam-Clay model, proposed by Borja and Tamagnini [41], it is known that the principal directions of $\left(\mathbf{C}_l^e\right)^{tr}$ are the same as the principal directions $\mathbf{n}_i, i=1,2,3$ of $\mathbf{C}_l^e$. Similarly, $\left(\hat{\mathbf{n}}\right)^{tr}$ is assumed to be the same as $\hat{\mathbf{n}}$. Therefore, the solution of

the plasticity equations is complete if ε_v^e and ε_s^e are determined along with the consistency parameter and the Kirchhoff pre-consolidation pressure parameter P_c.

As previously mentioned, the rate form of the constitutive equations can, in general, be used with other plasticity equations to define a set of differential equations that can be integrated using implicit integration methods or the return mapping algorithm. The plasticity equations presented in section 3.1 are typically solved in either an implicit or explicit fashion. The explicit solution, while easier, requires small time steps for stability. Implicit schemes are more computationally intensive, but are stable. Fairly small times steps may still be needed for accuracy. The number of equations that govern the behavior of the hyperelastic elastoplastic finite deformation Cam-Clay model [41] is much smaller than the number of equations required for solving a general plasticity problem. In this model, advantage is taken of the properties of the natural logarithms to formulate the flow rate equations in terms of elastic strain variables, thereby allowing for the use of empirical hardening formulas. If J is the determinant of the matrix of position vector gradients $\mathbf{J} = \mathbf{J}^e\mathbf{J}^p$, it follow that $J = J^e J^p$, where J^e and J^p are, respectively, the determinants of $\mathbf{J}^e$ and $\mathbf{J}^p$. Because $\varepsilon_v = \sum_{i=1}^{3} \ln(\lambda_i) = \ln(\lambda_1\lambda_2\lambda_3) = \ln(J)$, it follows that

$$\varepsilon_v = \ln\left(J^e J^p\right) = \ln\left(J^e\right) + \ln\left(J^p\right) = \varepsilon_v^e + \varepsilon_v^p \tag{37}$$

This relationship, upon differentiation, leads to the following rate form:

$$\dot{\varepsilon}_v = \frac{\dot{J}}{J} = \dot{\varepsilon}_v^e + \dot{\varepsilon}_v^p = \frac{\dot{J}^e}{J^e} + \frac{\dot{J}^p}{J^p} \tag{38}$$

In the Cam-Clay model of Borja and Tamagnini [41], the following hardening law is used:

$$\frac{v}{v_0} = \left(\frac{P_{c0}}{P_c}\right)^{\tilde{\lambda}} \tag{39}$$

In this equation, $v=(1+e)$ is the specific volume, e is the soil void ratio, $\tilde{\lambda}$ is a soil compressibility index, and subscript 0 refers to the reference configuration. Because $J=v/v_0$ and $\dot{J}=\dot{v}/v_0$, it follows that

$$\dot{\varepsilon}_v=\frac{\dot{J}}{J}=\dot{\varepsilon}_v^e+\dot{\varepsilon}_v^p=\frac{\dot{v}}{v}=-\tilde{\lambda}\frac{\dot{P}_c}{P_c} \tag{40}$$

In the special case of *virgin isotropic loading*, $\varepsilon_s^e=0$, and $P_c=P$. It follows then from Eq. 35 that $P_c=P_0e^{\Omega}$ and $\dot{P}_c=-(P_0/\hat{\kappa})e^{\Omega}\dot{\varepsilon}_v^e=-(P_c/\hat{\kappa})\dot{\varepsilon}_v^e$. Using this equation and Eq. 40, one obtains the following hardening law expressed in terms of $\dot{\varepsilon}_v^p$:

$$\frac{\dot{P}_c}{P_c}=-\Theta\dot{\varepsilon}_v^p,\quad \dot{\varepsilon}_v^p=\frac{\dot{J}^p}{J^p},\quad \Theta=\frac{1}{\hat{\lambda}-\hat{\kappa}} \tag{41}$$

It is also important to point out that on the *isotropic consolidation curve*, one has the equation $(\dot{v}/v)=-\hat{\lambda}(\dot{P}/P)$, and on the *swelling/recompression curves*, one has $(\dot{v}/v)=-\hat{\kappa}(\dot{P}/P)$. Finally, using the assumption of the associative plasticity, the discrete flow rule at time t_{n+1} for implicit time integration in the space defined by the elastic Eulerian logarithmic stretches can be written as

$$\boldsymbol{\varepsilon}_{n+1}^e=\left(\boldsymbol{\varepsilon}_{n+1}^e\right)^{tr}-\Delta\lambda_{n+1}\left.\frac{\partial f}{\partial\boldsymbol{\beta}}\right|_{n+1} \tag{42}$$

where $f=f(P,Q,P_c)=(Q^2/M^2)+P(P-P_c)$, $\left(\boldsymbol{\varepsilon}_{n+1}^e\right)^{tr}$ is the trial elastic strain, $\boldsymbol{\beta}$ is the vector of the principal values of the effective Kirchhoff stress tensor, and $\Delta\lambda$ is a plastic multiplier. The above equations can be shown to lead to the following set of equations that can be used to define a scalar return mapping algorithm [41] in the invariants of the elastic logarithmic stretches:

$$\left.\begin{aligned} &\varepsilon_v^e = \left(\varepsilon_v^e\right)^{tr} - \Delta\lambda \frac{\partial f}{\partial P}, \quad \varepsilon_s^e = \left(\varepsilon_s^e\right)^{tr} - \Delta\lambda \frac{\partial f}{\partial Q} \\ &f\left(P, Q, P_c\right) \le 0, \quad \Delta\lambda \ge 0, \quad \Delta\lambda f\left(P, Q, P_c\right) = 0 \end{aligned}\right\} \tag{43}$$

An example implicit integration scheme for the finite deformation Cam-Clay plasticity soil model can be developed by considering Eq. 43 as a set of simultaneous nonlinear equations. An application of the Newton-Raphson method can be used to solve this set of nonlinear equations. To this end, the residual vector $\mathbf{r}$ and the vector of unknowns $\mathbf{x}$ are written as follows:

$$\mathbf{r}^p = \begin{bmatrix} \varepsilon_v^e - \varepsilon_v^{e\ tr} + \Delta\lambda \dfrac{\partial f}{\partial P} \\ \varepsilon_s^e - \varepsilon_s^{e\ tr} + \Delta\lambda \dfrac{\partial f}{\partial Q} \\ f \end{bmatrix}, \quad \mathbf{x}^p = \begin{bmatrix} \varepsilon_v^e \\ \varepsilon_s^e \\ \Delta\lambda \end{bmatrix} \tag{44}$$

The Newton-Raphson solution procedure requires the iterative solution of the algebraic system $\left(\partial \mathbf{r}^p / \partial \mathbf{x}^p\right) \Delta \mathbf{x}^{p+1} = -\mathbf{r}^p$, where $\Delta \mathbf{x}^{p+1}$ is the vector of Newton differences. Having determined ε_v^e and $\dot{\varepsilon}_s^e$, the effective Kirchhoff pre-consolidation pressure P_c can be determined from the Cam-Clay hardening law. One can also determine $\boldsymbol{\varepsilon}^e = \varepsilon_v^e \boldsymbol{\delta} + \varepsilon_s^e \hat{\mathbf{n}}$. Using these elastic strain components, the principal values of $\mathbf{C}_l^e$ can be determined. Using these values and the principal directions, $\mathbf{n}_i, i = 1,2,3$, the tensor $\mathbf{C}_l^e$ can be calculated and stored for use in the next time step. A closed form expression for the consistent tangent operator $\left(\partial \mathbf{r}^p / \partial \mathbf{x}^p\right)$ can be found and the algorithm can be made more efficient by the application of the static condensation technique [41].

7.3 ANCF Challenges

The goal of using ANCF finite elements as the basis for the integration of continuum-based soil models and MBS algorithms is to develop a new computational framework for the systematic

and efficient simulations of wheeled and tracked vehicles. Nonetheless, there are several fundamental issues that need to be addressed in order to successfully develop such a new and integrated computational environment. Some of these fundamental issues are discussed below.

1. ANCF finite elements are classified as fully parameterized and gradient deficient finite elements. Fully parameterized elements employ complete set of coordinate lines, while gradient deficient elements do not employ a complete set of coordinate lines. Some of fully parameterized ANCF finite elements, as with other existing finite elements, may suffer from locking problems in the case of thin and stiff structures. In order to explain the source of the locking, it is helpful to distinguish between two fundamentally different sources of locking*; kinematic* and *stiffness*-produced locking. In the case of kinematics-produced locking, the ANCF interpolating polynomials used for some elements cannot assume shapes that are expected in response to loading conditions. This kinematic-produced locking can be encountered with any other polynomial-based FE formulations. For example, a first order approximation (straight line) cannot be used to capture bending regardless of the loading conditions. The problem of kinematic-produced locking can always be solved by developing a library of finite elements that employ interpolating functions that have different polynomial orders and different numbers and types of degrees of freedom. Research in the important area of *element technology* is, therefore, necessary in order to develop new ANCF finite elements that are suited for different applications.
2. The stiffness-produced locking, on the other hand, can be the result of very high stress forces in some directions. These high stress forces can be the result of high stiffness coefficients and/or the result of coupling between different modes of deformations. For

example, most existing beam formulations assume that the beam cross section remains rigid regardless of the type and magnitude of deformations and loadings. It is unrealistic, for example, to have a beam elongation without deformation in the beam cross section. This important Poisson mode of deformation can be systematically captured using ANCF beam elements. This is a unique and desirable feature despite the fact that such mode coupling can, in some applications, introduce very high frequencies and can lead to the deterioration of the element performance. The objective of the research in the area of element technology is to address these problems in order to develop new elements, force formulations, and integration schemes that provide accurate and efficient solutions for the stiffness-produced locking problems.

3. While fully parameterized ANCF finite elements allow the use of general continuum mechanics approach, these elements do not preclude using other elastic force formulations [109]. To further explain this important point, one may consider the trivial case of zero elastic forces, $\mathbf{Q}_s = \mathbf{0}$ (see Eq. 33). In this case, the equations of motion can be written as $\mathbf{M}\ddot{\mathbf{e}} = \mathbf{Q}_e$, where the vector $\mathbf{Q}_e$ is the nodal force vector that does not include any elastic restoring forces (zero stiffness). Because ANCF finite elements lead to a constant mass matrix, the LU factorization of the mass matrix $\mathbf{M}$ can be performed only once in advance. Even for very large systems, the ANCF equation $\mathbf{M}\ddot{\mathbf{e}} = \mathbf{Q}_e$ can be solved order of magnitude faster than real time. Therefore, the ANCF kinematic description (assumed displacement field) is not the source of the stiffness-produced locking. The formulation of the elastic forces is the source of the stiffness-produced locking. ANCF finite elements allow the use of elastic force formulations used in other

FE formulations and also allow for the use of the well-developed techniques documented in the FE literature to solve the locking problems.

4. Another issue that must be addressed when continuum-based soil models are integrated with ANCF/MBS algorithms is the dimensionality of the problem. ANCF finite elements employ more coordinates than what is normally used in conventional structural FE formulations. The increase in the dimensionality, however, allows, as previously mentioned, for capturing important deformation modes that cannot be captured using other FE formulations. Warping, for example, can be systematically captured using ANCF finite elements without the need for artificially introducing warping functions. Similarly, tapered structure geometry can be described exactly using ANCF finite elements without the need for using several stepping elements. It is also important to point out that the increase in dimensionality does not have the same adverse effect as the increase in the stiffness. Many existing numerical time integration techniques, particularly the explicit ones, are designed to efficiently solve very large systems, but these methods can fail in the case of stiff equations. While the problems associated with high stiffness and locking were previously discussed in this section, it is important to point out that ANCF finite elements can be used to develop new meshes that have constant mass matrix and linear connectivity conditions. An optimum sparse matrix structure of the equations of motion with minimum number of nonzero entries can always be obtained using ANCF finite elements. For example, for tracked vehicles as the one shown in Figure 11, the rigid-link chains of the vehicle have a highly nonlinear inertia matrix. The two chains of the vehicle shown in Figure 11 have 128 revolute (pin) joints that introduce 640 highly nonlinear algebraic equations. Using ANCF finite

elements, it is possible to develop a flexible-link chain model that has linear joint formulations, thereby eliminating the joint constraint equations at a preprocessing stage and reducing the number of nonzero elements by more than 12000 [110]. The dimension of the constraint formulations (constraint functions, Jacobian, and first and second derivative vectors), used at the position, velocity, and acceleration steps, and the number of nonzero entries resulting from the constraint formulation are significantly reduced. Additionally, by using Cholesky coordinates, the inertia matrix reduces to an identity matrix. This allows for developing efficient flexible-link chain tracked vehicle models that capture significant details that cannot be captured using previously developed vehicle models.

5. Capturing geometric details can be important when the analysis is performed. This may require, in some applications, the use of a larger number of finite elements. This can lead to an increase in the dimensionality of the problem. While the dimensionality problem is an issue that must be addressed, as previously discussed in this section, it became recently clear that the use of geometrically correct finite elements is necessary. All existing structural finite elements (conventional elements that employ infinitesimal rotations and large rotation vector formulation elements) lead to geometric distortion, and this is the reason that such elements are being now abandoned. When using these elements as the basis for analysis, CAD models cannot be converted to analysis meshes without geometry distortion. Furthermore, there is no linear mapping between such elements and CAD representations developed using B-splines and NURBS geometries. B-spline and NURBS representations, on the other hand, can be converted to ANCF meshes without geometric distortion. This allows for developing accurate tire and

uneven terrain geometries using ANCF finite elements, thereby facilitating the integration of solid CAD modeling and analysis.

8. SUMMARY

In this paper, soil mechanics formulations that can be integrated with FE/MBS algorithms to study vehicle dynamics are reviewed. Several simple models including analytical terramechanics models are discussed. Bekker's model as well as other parametric and analytical terramechanics models have been used in the study of track/soil interaction and can be implemented in MBS algorithms using simple discrete force elements. These simple models, however, have serious limitations because they do not capture the distributed elasticity and plasticity of the soil. The advantages and limitations of the discrete element method (DEM) are also discussed in this paper. More general continuum plasticity soil formulations are reviewed. Among the continuum soil plasticity formulations discussed in this paper are the Mohr-Coulomb, Drucker-Prager, modified Cam-Clay, Barcelona Basic, elasto-plastic cap model for partially saturated soil, viscoplastic cap, and bounding surface plasticity unsaturated models. The integration algorithm that is commonly used to solve the plasticity equations is discussed. This algorithm can be integrated within the absolute nodal coordinate formulation (ANCF) to develop a computational procedure that allows for the study of vehicle/soil interaction dynamics. The ANCF/soil model integration will be the subject of future investigations.

ACKNOWLEDGEMENTS

This research was supported by the US Army Tank-Automotive Research, Development, and Engineering Center (TARDEC) (Contract # W911NF-07-D-0001).

REFERENCES

[1] Whitlow, R., 1995, *Basic Soil Mechanics*, John Wiley & Sons Inc., New York.

[2] Maugin, G.A., 1992, *The Thermomechanics of Plasticity and Fracture*, Cambridge University Press, Cambridge.

[3] Wong, J.Y., 2010, *Terramechanics and Off-Road Vehicle Engineering*, Elsevier, Oxford, UK.

[4] Bekker, M.G., 1969, *Introduction to Terrain-Vehicle Systems*, The University of Michigan Press, Ann Arbor.

[5] Priddy, J.D., and Willoughby, W.E., 2006, "Clarification of Vehicle Cone Index with Reference to Mean Maximum Pressure", *Journal of Terramechanics*, 43, pp. 85-96.

[6] Schmid, I.C., 1995, "Interaction of Vehicle and Terrain Results from 10 Years Research at IKK", *Journal of Terramechanics,* 32, pp. 3-26.

[7] Ryu, H.S., Huh, K.S., Bae, D.S., and Choi, J.H., 2003, "Development of a Multibody Dynamics Simulation Tool for Tracked Vehicles (Part I, Efficient Contact and Nonlinear Dynamic Modeling)", *JSME International Journal Series C*, 46(2), pp. 540-549.

[8] Garber, M., and Wong, J.Y., 1981, "Prediction of Ground Pressure Distribution Under Tracked Vehicles – Part I. An Analytical Method for Predicting Ground Pressure Distribution", *Journal of Terramechanics*, 18(1), pp.1–23.

[9] Okello, J.A., 1994, "Prediction and Experimental Validation of the Field Tractive Performance of a Rubber Track Unit", *Journal of Agricultural Engineering International,* 59, pp. 163-171.

[10] Okello, J.A., 1998, "A Theoretical and Experimental Investigation of Rubber Track Performance Models", *Journal of Agricultural Engineering International,* 69, pp. 15-24.

[11] Rubinstein, D., and Coppock, J.L., 2007, "A Detailed Single-Link Track Model for Multi-Body Dynamic Simulation of Crawlers", *Journal of Terramechanics*, 4(4), pp. 355–364.

[12] Park, W.Y., Chang, Y.C., Lee, S.S., Hong, J.H., Park, J.G., and Lee, K.S., 2008, "Prediction of the Tractive Performance of a Flexible Tracked Vehicle", *Journal of Terramechanics*, 45, pp. 13–23.

[13] Mao, S.G., and Han, R.P.S., 2008, "Nonlinear Complementarity Equations for Modeling Tire-Soil Interaction -An Incremental Bekker Approach", *Journal of Sound and Vibration,* 312, pp. 380-398.

[14] Sandu, C., Worley, M.E., and Morgan, J.P., 2010, "Experimental Study on the Contact Patch Pressure and Sinkage of a Lightweight Vehicle on Sand", *Journal of Terramechanics*, 47, pp. 343–359.

[15] Schwanghart, H., 1991, "Measurement of Contact Area, Contact Pressure and Compaction under Tires in Soft Soil", *Journal of Terramechanics*, 28(4), pp. 309-318.

[16] Reece, A.R., 1965, "Principles of Soil-Vehicle Mechanics", Proceedings of the Institution of Mechanical Engineers, Automobile Division, 180(2A), pp. 45-66.

[17] Sandu, C., Sandu, A., Chan, B.J., and Ahmadian, M., 2004, "Treating Uncertainties in Multibody Dynamic Systems using a Polynomial Chaos Spectral Decomposition", Proceedings of the ASME IMECE 2004, sixth annual symposium on "Advanced Vehicle Technology", November 14-19, Anaheim, CA.

[18] Irani, R.A., Bauer, R.J, and Warkentin, A., 2011, "A Dynamic Terramechanic Model for Small Lightweight Vehicles with Rigid Wheels and Grousers Operating in Sandy Soil", *Journal of Terramechanics,* 48, pp. 307-318.

[19] Fossum, A.F., and Brannon, R.M., 2004, "The Sandia Geomodel: Theory and User's Guide", Technical Report, Sandia National Laboratories, Albuquerque, NM and Livermore, CA.

[20] de Souza Neto, E.A., Peric, D., and Owen, D.R.J, 2008, *Computational Methods for Plasticity*, John Wiley & Sons Ltd, West Sussex, UK.

[21] Araya, K., and Gao, R., 1995, "A Non-Linear Three-Dimensional Finite Element Analysis of Subsoiler Cutting with Pressurized Air Injection", *Journal of Agricultural Engineering Research*, 61, pp. 115-128.

[22] Mouazen, A.M., and Nemenyi, M., 1999, "Finite Element Analysis of Subsoiler Cutting in Non-homogeneous Sandy Loam Soil", *Soil and Tillage Research,* 51, pp. 1-15.

[23] Rudnicki, J.W., and Rice, J.R., 1975, "Conditions for Localization of Deformation in Pressure-Sensitive Dilatant Materials", *Journal of the Mechanics and Physics of Solids*, 23(6), pp. 371-394.

[24] Scott, R., 1985, "Plasticity and Constitutive Relations in Soil Mechanics", *Journal of Geotechnical Engineering*, 111(5), pp. 559-605.

[25] Goldscheider, M., 1982, "True Triaxial Tests on Dense Sands", Results of the International Workshop on Constitutive Relations for Soils, June 9, Balkema, Rotterdam.

[26] An, J., 2010, "Soil Behavior under Blast Loading", Ph.D. Dissertation, The University of Nebraska.

[27] Seta, E., Kamegawa, T., and Nakajima, Y., 2003, "Prediction of Snow/Tire Interaction using Explicit FEM and FVM", *Tire Science and Technology,* 31(3), pp. 173-188.

[28] Drucker, D.C., Greenberg, J., and Prager, W., 1952, "Extended Limit Design Theorems for Continuous Media", *Quarterly of Applied Mathematics*, 9, pp. 381-389.

[29] Vermeer, P.A., and De Borst, R., 1984, "Non-associated Plasticity for Soils, Concrete, and Rock", *Heron,* 29(3), pp.1-64.

[30] DiMaggio, F.L., and Sandler, I.S., 1971, "Material Model for Granular Soils", *Journal of the Engineering Mechanics Division*, 97(EM3), pp. 935-950.

[31] Matsuoka, H., and Nakai, T., 1974, "Stress-Deformation and Strength Characteristics of Soil under Three Different Principal Stresses", Proceedings of the Japanese Society of Civil Engineers, 232, pp. 59-70.

[32] Brinkgreve, R.B.J., 2005, "Selection of Soil Models and Parameters for Geotechnical Engineering Application", Soil Constitutive Models: Evaluation, Selection, and Calibration, Geo-frontier Conference of ASCE*,* January 24 – 25, Austin, Texas, pp. 69-98.

[33] Xia, K., 2011, "Finite element modeling of tire/terrain interaction: Application to Predicting Soil Compaction and Tire Mobility", *Journal of Terramechanics,* 48(2), pp. 113-123.

[34] Lee, J.H., 2011, "Finite Element Modeling of Interfacial Forces and Contact Stresses of Pneumatic Tire on Fresh Snow for Combined Longitudinal and Lateral Slips", *Journal of Terramechanics,* 48, pp. 171-197.

[35] Fassbender, F.R., Fervers, C.W., and Harnisch, C., 1997, "Approaches to Predict the Vehicle Dynamics of Soft Soil", *International Journal of Vehicle Mechanics and Mobility*, 27, pp. 173-188.

[36] Meschke, G., Liu, C., and Mang, H.A., 1996, "Large Strain Finite-Element Analysis of Snow", *Journal of Engineering Mechanics*, 122, pp. 591-602.

[37] Gudehus, G., 1973, "Elastoplastiche Stoffgleichungen Guer Trockenen Sand", *lngenieur-Archiv*, 42(3), pp. 151-169.

[38] William, K.J. and Warnke, E.P., 1975, "Constitutive Model for Triaxial Behavior of Concrete", ISMES Seminar on Concrete Structures to Triaxial Stresses, Bergamo, Italy, pp. 1-30.

[39] Wood, D.M., 1990, *Soil Behaviour and Critical State Soil Mechanics*, Cambridge University Press, Cambridge.

[40] Roscoe, K.H., and Burland, J.B., 1968, "On the Generalized Stress-Strain Behaviour of Wet Clay", *Engineering Plasticity*, J. Heymann, F.A. Leckie (Eds.), pp. 535-609, Cambridge University Press, Cambridge.

[41] Borja, R.I., and Tamagnini, C., 1996, "Cam-Clay Plasticity, Part III: Extension of the Infinitesimal Model to Include Finite Strains", *Computer Methods in Applied Mechanics and Engineering*, 155, pp.73-95.

[42] Karim, M.R., and Gnanendran, C.T., 2008, "Review of Visco-Plastic Soil Models for Predicting the Performance of Embankments on Soft Soils", The 12th International Conference of International Association for Computer Methods and Advances in Geomechanics, October 1-6, Goa, India.

[43] Berli, M., Kirby, J.M., Springman, S.M., and Schulin, R., 2003, "Modeling Compaction of Agricultural Subsoils by Tracked Heavy Construction Machinery under Various Moisture Conditions in Switzerland", *Soil and Tillage Research*, 73, pp. 57-66.

[44] Bryson, L. S., and Salehian, A., 2011, "Performance of Constitutive Models in Predicting Behavior of Remolded Clay", *Acta Geotechnica*, 6, pp. 143-154.

[45] Masin, D., Tamagnini, C., Viggiani, G., and Costanzo, D., 2006, "Directional Response of a Reconstituted Fine-Grained Soil Part II: Performance of Different Constitutive Models", *International Journal for Numerical and Analytical Methods in Geomechanics*, 30(1), pp. 1303-1336.

[46] McDowell, G.R., and Hau, K.W., 2004, "A Generalized Modified Cam Clay Model for Clay and Sand", *Granular Matter*, 1, pp. 11-16.

[47] Drucker, D.C., Gibson, R.E., and Henkel, D.J., 1957, "Soil Mechanics and Work Hardening Theories of Plasticity", *Transactions of the American Society of Civil Engineers*, 122, pp. 338-346.

[48] Chen, W.F., and Baladi, G.Y., 1985, *Soil Plasticity: Theory and Implementation*, Elsevier, Amsterdam.

[49] Sandler, I.S., and Rubin, D., 1979, "An Algorithm and a Modular Subroutine for the Cap Model", *International Journal for Numerical and Analytical Methods in Geomechanics*, 3, pp. 173-186.

[50] Simo, J.C., Ju, J.W., Pister, K.S., and Taylor, R.L., 1988, "Assessment of Cap Model: Consistent Return Algorithms and Rate-dependent Extension", *Journal of Engineering Mechanics, ASCE*, 114(2), pp. 191-218.

[51] Foster, C.D., Regueiro, R.A., Fossum, A.F., and Borja, R.I., 2005, "Implicit Numerical Integration of a Three-Invariant, Isotropic/Kinematic Hardening Cap Plasticity Model for Geomaterials", *Computer Methods in Applied Mechanics and Engineering*, 194(50-52), pp. 5109-5138.

[52] Brannon, R.M., Fossum, A.F., and Strack, O.E., 2009, "KAYENTA: Theory and User's Guide", Sandia Report SAND2009-2282.

[53] Wan, R.G., and Guo, P.J., 2001, "Drained Cyclic Behavior of Sand with Fabric Dependence", *Journal of Engineering Mechanics*, 127(11), pp. 1106-1116.

[54] Whittle, A.J., and Kavvadas, M.J., 1994, "Formulation of MIT-E3 Constitutive Model for Overconsolidated Clays", *Journal of Geotechnical Engineering*, 120(1), pp. 173-198.

[55] Wheeler, S.J., Naatanen, A., Karstunen, M., and Lojander, M., 2003, "An Anisotropic Elastoplastic Model for Soft Clays", *Canadian Geotechnical Journal*, 40, pp. 403-418.

[56] Perzyna, P., 1966, "Fundamental Problems in Viscoplasticity", *Advances in Applied Mechanics,* 9, pp. 243-377.

[57] Lorefice, R., Etse, G., and Carol, I., 2008, "Viscoplastic Approach for Rate-dependent Failure Analysis of Concrete Joints and Interfaces", *International Journal of Solids and Structures*, 45, pp. 2686-2705.

[58] Darabi, M.K., Abu Al-Rub, R.K., Masad, E.A., and Little, D.N., 2011, "Thermodynamic-Based Model for Coupling Temperature-Dependent Viscoelastic, Viscoplastic, and Viscodamage Constitutive Behavior of Asphalt Mixtures", *International Journal for Numerical and Analytical Methods in Geomechanics*, 48(1), pp. 191-207.

[59] Katona, M.G., 1984, "Verification of Viscoplastic Cap Model", *Journal of Geotechnical Engineering*, 110(8), pp. 1106-1125.

[60] Tong, X., and Tuan, C.Y., 2007, "Viscoplastic Cap Model for Soils under High Strain Rate Loading", *Journal of Geotechnical and Geoenvironmental Engineering,* 133(2), pp. 206-214.

[61] Liu, H., and Ling, H.I., 2007, "Unified Elastoplastic-Viscoplastic Bounding Surface Model of Geosynthetics and its Applications to Geosynthetic Reinforced Soil-Retaining Wall Analysis", *Journal of Engineering Mechanics,* 133(7), pp. 801-814.

[62] Yin, J.H., and Graham, J., 1999, "Elastic Viscoplastic Modeling of the Time Dependent Stress–Strain Behavior of Soils", *Canadian Geotechnical Journal,* 36, pp. 736-745.

[63] Simo, J.C., and Hughes, T.J.R., 1998, *Computational Inelasticity*, Springer Verlag, New York.

[64] Duvaut, G., and Lions, J.L., 1972, "Les Inequations en Mechanique et en Physique", Dunod, *Travaux et Recherches,* 21.

[65] Abdullah, W.S., 2011, "Viscoplastic Finite Element Analysis of Complex Geotechnical Problems", *Jordan Journal of Civil Engineering*, 5(2), pp. 302-314.

[66] Saliba, J.E., 1990, "Elastic-Viscoplastic Finite Element Program for Modeling Tire-Soil Interaction", *Journal of Aircraft*, 27(4), pp.350-357.

[67] Brezzi, F., 1990, "A Discourse on the Stability Conditions for Mixed Finite Element Formulations", *Computer Methods in Applied Mechanics and Engineering*, 82(1-3), pp. 27-57.

[68] White, J.A., and Borja, R.I., 2008, "Stabilized Low-Order Finite Elements for Coupled Solid-Deformation/Fluid Diffusion and their Application to Fault Zone

Transients", *Computer Methods in Applied Mechanics and Engineering,* 197(49-50), pp. 4353-4366.

[69] Alonso, E.E., Gens, A., and Josa, A., 1990, "A Constitutive Model for Partially Saturated Soils", *Geotechnique*, 46(2), pp. 405-430.

[70] Kohler, R., 2007, "Numerical Modeling of Partially Saturated Soils in the Context of a Three-Phase FE-Formulation", Ph.D. Dissertation, University of Innsbruck.

[71] Dafalias, Y.F., and Popov, E., 1976, "Plastic Internal Variables Formalism of Cyclic Plasticity", *Journal of Applied Mechanics*, 98(4), pp. 645-651.

[72] Dafalias, Y.F., and Herrmann, L.R., 1982, "Bounding Surface Formulation of Soil and Cyclic Loads", Soil Mechanics-Transient and Cyclic Loads, G.N. Pande, O.C. Zienkiewicz (Eds.), Wiley, London.

[73] McVay, M., and Taesiri, Y., 1985, "Cyclic Behavior of Pavement Base Materials", *Journal of Geotechnical Engineering Div. ASCE*, 111(1), pp. 399-416.

[74] Hashiguchi, K., and Ueno, M., 1977, "Elastic-Plastic Constitutive Laws of Granular Materials", Proceedings of the 9th International Conference on Soil mechanics and Foundation Engineering, July 10 – 15,Tokyo, Japan.

[75] Aboim, C.A., and Roth, W.H., 1982, "Bounding Surface Plasticity Applied to Cyclic Loading of Sand", Proceedings of the International Symposium on Numerical Models, September, Zurich, Switzerland, pp. 65-72.

[76] Bardet, J.P., 1985, "Application of Bounding Surface Plasticity to Cyclic Sand Behavior", Proceedings of the 2nd International Conference on Soil Dynamics and Earthquake Engineering, pp. 3-16.

[77] Wong, H., Morvan, M., and Branque, D., 2009, "A 13-parameter Model for Unsaturated Soil Based on Bounding Surface Plasticity", *Journal of Rock Mechanics and Geotechnical Engineering.*, 2(2), pp. 135-142.

[78] Belytschlo, T., Liu, W.K., Moran, B., 2000, *Nonlinear Finite Elements for Continua and Structures*, Wiley, Chichester, New York.

[79] Li, S., and Liu, W.K., 2002, "Meshfree and Particle Methods and their Applications", *Applied Mechanics Reviews*, 55(1), pp. 1-34.

[80] Tutumluer, E., Huang, H., Hashash, Y., and Ghaboussi, J., 2006, "Aggregate Shape Effects on Ballast Tamping and Railroad Track Lateral Stability", AREMA Annual Conference, September 17-20, Loisville, Kentucky.

[81] Reeves, T., Biggers, S., Joseph, P., Summers, J.D., and Ma, J., 2010, "Exploration of Discrete Element Method to Dynamically Model Sandy Terrain", SAE 2010 World Congress & Exhibition, April 12-15, Detroit, Michigan, pp. 67-74.

[82] Knuth, M.A., Johnson, J.B., Hopkins, M.A., Sullivan, R.J. and Moore, J.M., 2012, "Discrete Element Modeling of a Mars Exploration Rover Wheel in Granular Material", *Journal of Terramechanics*, 49, pp. 27-36.

[83] Oida, A., and Momozu, M., 2002, "Simulation of Soil Behavior and Reaction by Machine Part by Means of DEM", *Agricultural Engineering International: the CIGR Journal of Scientific Research and Development,* PM 01 004, 4, pp. 1-7.

[84] Khulief, Y.A., and Shabana, A.A., 1987, "A Continuous Force Model for the Impact Analysis of Flexible Multi-Body Systems", *Mechanism and Machine Theory*, 22(3), pp. 213-224.

[85] Asaf, Z., Rubinstein, D., and Shmulevich, I., 2006, "Evaluation of Link-Track Performances using DEM", *Journal of Terramechanics*, 43(2), pp. 141-161.

[86] Nakashima, H., Fujii, H., Oida, A., Momozu, M., Kanamori, H., Aoki, S., Yokoyama, T., Shimizu, H., Miyasaka, J., and Ohdoi, K., 2010, "Discrete Element Method Analysis of Single Wheel Performance for a Small Lunar Rover on Sloped Terrain", *Journal of Terramechanics*, 47, pp. 307-321.

[87] Li, W., Huang, Y., Cui, Y., Dong, S., and Wang, J., 2010, "Trafficability Analysis of Lunar Mare Terrain by Means of the Discrete Element Method for Wheeled Rover Locomotion", *Journal of Terramechanics*, 47, pp. 161-172.

[88] Bui, H.H., Fukagawa, R., Sako, K., and Ohno, S., 2008, "Lagrangian Meshfree Particle Method (SPH) for Large Deformation and Failure Flows of Geomaterial using Elastic-Plastic Soil Constitutive Model", *International Journal for Numerical and Analytical Methods in Geomechanics*, 32, pp. 1537-1570.

[89] Chen, J.S., Pan, C., and Wu, C.T., 1997, "Large Deformation Analysis of Rubber based on a Reproducing Kernel Particle Method", *Computational Mechanics*, 19, pp. 211-227.

[90] Nakashima, H., and Oida, A., 2004, "Algorithm and Implementation of Soil-Tire Contact Analysis Code based on Dynamic FE-DE Method", *Journal of Terramechanics*, 41, pp. 127-137.

[91] El-Gindy, M., Lescoe, R., Oijer, F., Johansson, I., and Trivedl, M., 2011, "Soil Modeling using FEA and SPH Techniques for a Tire-Soil Interaction", Proceedings of the ASME 2011 IDET/CIE, August 28-31, Washington, DC.

[92] Lescoe, R., El-Gindy, M., Koudela, K., 2010, "Tire-Soil Modeling using Finite Element Analysis and Smooth Particle Hydrodynamics Techniques", Proceedings of the 12th International Conference on Advanced Vehicle and Tire Technologies, August 15-18, Montreal, Canada, 4, pp. 3-18.

[93] Shoop, S.A., 2001, "Finite Element Modeling of Tire-Terrain Interaction", U.S. Army Corps of Engineers, Engineering Research and Development Center, Technical Report ERDC/CRREL TR-01-16.

[94] Chi, L., and Tessier, S., 1995, "Finite Element Analysis of Soil Compaction Reduction with High Flotation Tires", Proceedings of the 5th North American Conference of the ISTVS, Saskatoon, Saskatchewan, Canada, pp. 167-176.

[95] Ding, L., Deng, Z., Gao, K., Nagatani, K., and Yoshida, K., 2011, "Planetary Rovers' Wheel-Soil Interaction Mechanics: New Challenges and Applications for Wheeled Mobile Robots", *Intelligent Service Robotics*, 4(1), pp. 17-38.

[96] Azimi, A., Hirschkorn, M., Ghotbi, B.J., Kovecses, J., Angeles, J., Radziszewski, P., Tiechmann, M., Courchnesne, M., and Gonthier, Y., 2010, "Simulation-Based Rover Performance Evaluation and Effects of Terrain Modeling", In Proceedings of CASI Astronautics Conference ASTRO 2010, May 4-6.

[97] Liu, C.H., and Wong, J.Y., 1996, "Numerical Simulations of Tire-Soil Interaction Based on Critical State Soil Mechanics", *Journal of Terramechanics*, 33(5), pp. 209-221.

[98] Grujicic, M., Bell, W.C., Arakere, G., and Haque, I., 2009, "Finite Element Analysis of the Effect of Ep-Armouring on the Off-Road Braking and Sharp-Turn Performance of a High-Mobility Multi-Purpose Wheeled Vehicle", *Proceedings of the Institution of*

Mechanical Engineers, Part D: Journal of Automobile Engineering, 223(11), pp. 1419-1434.

[99] Xia, K., and Yang, Y., 2012, "Three-Dimensional Finite Element Modeling of Tire/Ground Interaction", *International Journal for Numerical and Analytical Methods in Geomechanics,* 36(4), pp. 498-516.

[100] Hambleton, J.P., and Drescher, A., 2009, "On Modeling a Rolling Wheel in the Presence of Plastic Deformation as a Three-or Two-Dimensional Process", *International Journal of Mechanical Sciences,* 51(11), pp. 846-855.

[101] Nankali, N., Namjoo, M., and Maleki, M.R., 2012, "Stress Analysis of Tractor Tire Interaction with Soft Soil using 2D Finite Element Method", *International Journal of Advanced Design and Manufacturing Technology,* 5(3), pp. 107-111.

[102] Shoop, S.A., Kestler, K., and Haehnel, R., 2006, "Finite Element Modeling of Tires on Snow", *Tire science and technology,* 34(1), pp. 2-37.

[103] Pruiksma, J.P., Kruse,G.A.M.,Teunissen, J.A.M.,and van Winnendael, M.F.P., 2011, "Tractive Performance Modelling of the Exomars Rover Wheel Design on Loosely Packed Soil Using the Coupled EulerianLagrangian Finite Element Technique", 11th Symposium on Advanced Space Technologies in Robotics and Automation, 12-14 April, Noordwijk, The Netherlands.

[104] Mohsenimanesh, A., Ward, S.M., Owende, P.O.M., and Javadi, A., 2009, "Modelling of Pneumatic Tractor Tyre Interaction with Multi-Layered Soil", *Biosystems Engineering,* 104(2), pp. 191-198.

[105] Carter, J.P., Booker, J.R., and Wroth, P., 1982, "A Critical State Soil Model for Cyclic Loading", Soil Mechanics –Transient and Cyclic Loads, G.N. Pande, O.C. Zienkewicz (Eds.), Wiley, London, pp. 219-252.

[106] Shabana, A.A., 2012, Computational Continuum Mechanics, 2nd Edition, Cambridge University Press, Cambridge, UK.

[107] Shabana, A.A., 2005, *Dynamics of Multibody Systems*, 3rd Edition, Cambridge University Press, Cambridge, UK.

[108] Shabana, A.A., 1998, "Computer Implementation of the Absolute Nodal Coordinate Formulation for Flexible Multibody Dynamics", *Nonlinear Dynamics*, Vol. 16, No. 3, July 1998, pp. 293-306.

[109] Nachbagauer, K., 2012, "Development of Shear and Cross Section Deformable Beam Finite Elements Applied to Large Deformation and Dynamic Problems", Ph.D. Dissertation, Johannes Kepler University, Lenz, Austria.

[110] Shabana, A.A., Hamed, A.M., Mohamed, A.A., Jayakumar, P., and Letherwood, M.D., 2012, "Use of B-Spline in the Finite Element Analysis: Comparison with ANCF Geometry", *ASME Journal of Computational and Nonlinear Dynamics*, Vol. 7(1), pp. 011008-1 – 011008-8.

[111] Carter, J.P., Booker, J.R., and Wroth, C.P., 1979, "A Critical State Soil Model For Cyclic Loading", Research Report No. CE 6, Monograph.

[112] Liu, C. H., Wong, J.Y., and Mang, H.A., 2000, "Large Strain Finite Element Analysis of Sand: Model, Algorithm and Application to Numerical Simulation of Tire–Sand Interaction", *Computers & Structures*, 74(3), pp. 253-265.

[113] Fervers, C.W., 2004, "Improved FEM Simulation Model for Tire–Soil Interaction", *Journal of Terramechanics,* 41(2), pp. 87-100.

[114] Haehnel, R.B., and Shoop, S.A., 2004, "A Macroscale Model for Low Density Snow Subjected to Rapid Loading", *Cold regions science and technology,* 40(3), pp. 193-211.

[115] Chiroux, R.C., Foster, W.A., Johnson, C.E., Shoop, S.A., and Raper, R.L., 2005, "Three-Dimensional Finite Element Analysis of Soil Interaction with a Rigid Wheel", *Applied mathematics and computation,* 162(2), pp. 707-722.

[116] Hambleton, J.P., and Drescher, A., 2008, "Modeling wheel-Induced Rutting in Soils: Indentation", *Journal of Terramechanics,* 45(6), pp. 201-211.

[117] Hambleton, J.P., and Drescher, A., 2009, "Modeling Wheel-Induced Rutting in Soils: Rolling", *Journal of Terramechanics,* 46(2), pp. 35-47.

[118] Grujicic, M., Marvi, H., Arakere, G., and Haque, I., 2010, "A Finite Element Analysis of Pneumatic-Tire/Sand Interactions during Off-Road Vehicle Travel", *Multidiscipline Modeling in Materials and Structures,* 6(2), pp. 284-308.

[119] Li, H., and Schindler, C., 2012, "Three-Dimensional Finite Element and Analytical Modelling of Tyre–Soil Interaction.", *Proceedings of the Institution of Mechanical Engineers, Part K: Journal of Multi-body Dynamics*.

[120] Li, H., and Schindler, C., 2012, "Application of Analytical and Finite Element Method in Tyre–Soil Modelling", *International Journal of Heavy Vehicle Systems,*19(4), pp. 333-354.

LIST OF TABLE CAPTIONS

LIST OF FIGURE CAPTIONS

1. Response of soil with respect to shearing [1,2]
2. Stress at a point R units away from the point load [3]
3. Contact area under a circular loading area [3]
4. Stress at a point due to a rectangular loading area [3]
5. Idealized flexible track and terrain interaction [3]
6. General yield function and return mapping
7. Failure surfaces in principal stress space [32]
8. The Modified Cam-Clay model [111]
9. Yield surface for Cap Model [70]
10. Yield surface of the extended cap model in terms of net stress and matric suction [70]
11. Tracked vehicle model

Category	Soil Model	Hardening	Nonlinear Pressure Dependence	Cyclic Loading	Unsaturated Soil	Fracture	Nonlinear Compressibility Law
Continuum Based Models in Standard Finite Element	Mohr-Coulomb	✓					
	Drucker-Prager	✓					
	Modified Cam-Clay	✓	✓	✓			✓
	Elasto-Plastic Cap Model for Partially Saturated Soils	✓	✓				✓
	Visco-Plastic Cap Model	✓	✓				
	Bounding Surface Plasticity Unsaturated Soil Model	✓	✓	✓	✓		
	Elasto-Plastic Barcelona Basic Model	✓	✓	✓	✓		
Terramechanics Models	Bekker's Soil Model			✓			
	Modified Bekker Soil Model	✓		✓			
Particle and Meshfree Models	Discrete Element Method		✓	✓	with modifications	✓	
	Meshfree	CM	CM	CM	CM	✓	CM

Table_1.tif

Reference	Software	Dimension	Model Type	Soil Model	Multilayered Soil?	Tire Model	Model the Tread?	Multi-Layered Tire?
[112]	MARC	2D	Wheel-Sand	Critical State Soil	No	Rigid	No	No
[93]	ABAQUS/Standard and /Explicit	3D	Wheel-Snow	Modified Drucker-Prager/Cap and Crushable Foam Model	No	Rigid and Modal Analysis	Yes, in Modal Analysis Tire	No
[113]	ABAQUS	2D	Tire-Soil	Modified Drucker-Prager/Cap	No	Flexible (force-deflection relation)	No	Yes
[114]	ABAQUS	3D	Wheel-Snow	Modified Drucker-Prager/Cap	No	Rigid	No	No
[115]	ABAQUS/Explicit	3D	Wheel-Soil	Modified Drucker-Prager/Cap	No	Rigid	No	No
[102]	ABAQUS/Explicit	3D	Tire-Snow	Modified Drucker-Prager/Cap	No	Modal Analysis	Yes	No
[116]	ABAQUS/Explicit	2D/3D	Wheel-Soil	Modified Drucker-Prager/Cap	No	Rigid	No	No
[117]	ABAQUS/Explicit	3D	Wheel-Soil	Modified Drucker-Prager/Cap	No	Rigid	No	No
[98]	ABAQUS	3D	Vehicle-Soil	CU-ARL Sand Model	No	Hyperelastic Blatz-Ko	Yes	No
[104]	ANSYS	3D	Tire-Soil	Linear and Bilinear Elastic	Yes	Hyperelastic Mooney-Rivlin	Yes	Yes
[100]	ABAQUS/Explicit	2D/3D	Wheel-Soil	Linear Elastic Von Mises	No	Rigid	No	No
[118]	ABAQUS	3D	Tire-Sand	CU-ARL Sand Model	No	Hyperelastic and Viscoelastic	Yes	Yes
[92]	PAM-SHOCK and PAM-CRASH	3D	Tire-Soil	Critical State Soil	No	Rigid and FE	Yes, in FE Tire	Yes, in FE Tire
[34]	ABAQUS/Explicit	3D	Tire-snow	Modified Drucker-Prager/Cap	No	Hyperelastic Mooney-Rivlin and Viscoelastic	No	Yes
[33]	see 2012 paper	3D	Tire-Soil	Modified Drucker-Prager/Cap	Yes	Nearly Incompressible Hyperelastic	No	Yes
[103]	ABAQUS/Explicit	3D	Tire-Lunar Soil	Critical State Soil and Drucker Prager shear failure Model	No	Linear Elastic	N.A.	Yes
[119]	ABAQUS	3D	Tire-Soil	Modified Drucker-Prager/Cap	No	Hyperelastic	Yes	Yes
[101]	ANSYS	2D	Tire-Soil	Modified Drucker-Prager/Cap	No	Hyperelastic Mooney-Rivlin	Yes	Yes
[120]	ABAQUS	3D	Tire-Sand	Modified Drucker-Prager/Cap	No	Hyperelasti NeoHookean	Yes	Yes
[99]	ABAQUS	3D	Tire-Soil and Four Tire-Soil	Modified Drucker-Prager/Cap	Yes	Hyperelastic	No	Yes

Table_2.tif

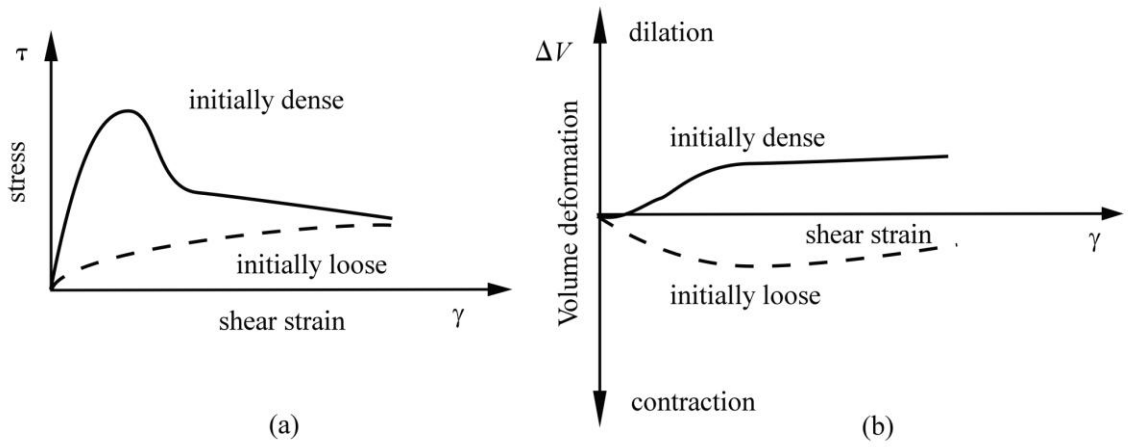
τ
stress
initially dense
initially loose
shear strain
γ
(a)
ΔV
dilation
Volume deformation
initially dense
shear strain
γ
initially loose
contraction
(b)

Fig_1.tif

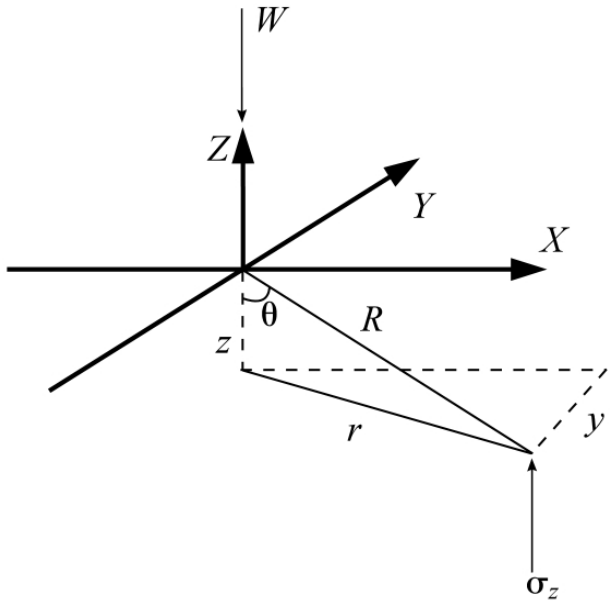

Fig_2.tif

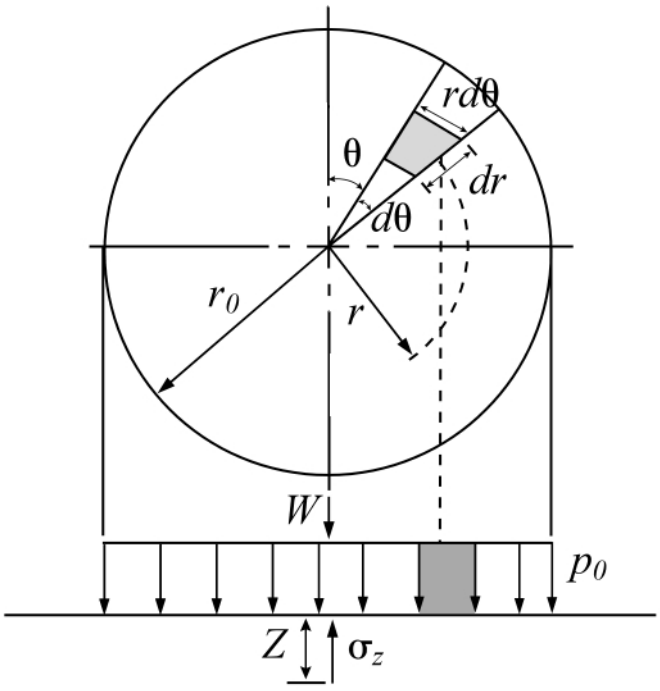

Fig_3.tif

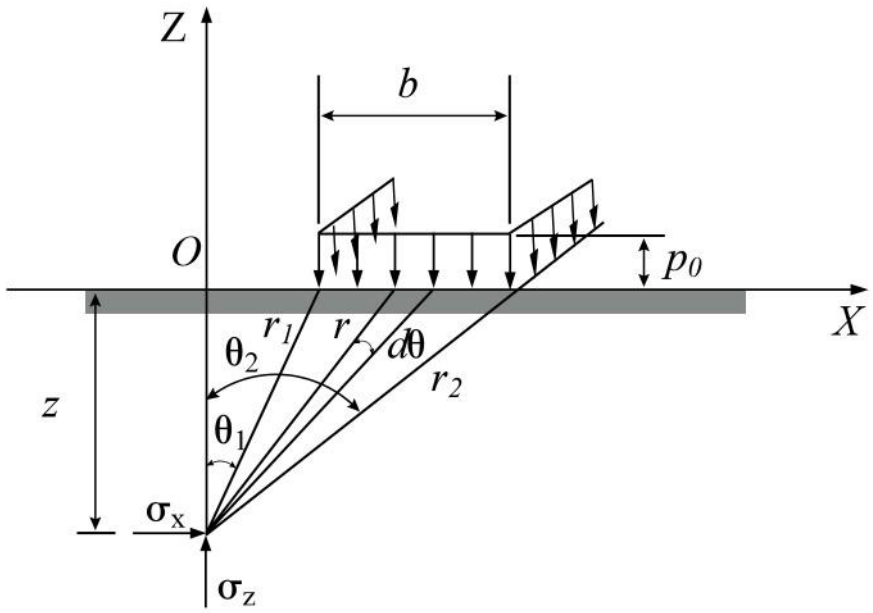

Fig_4.tif

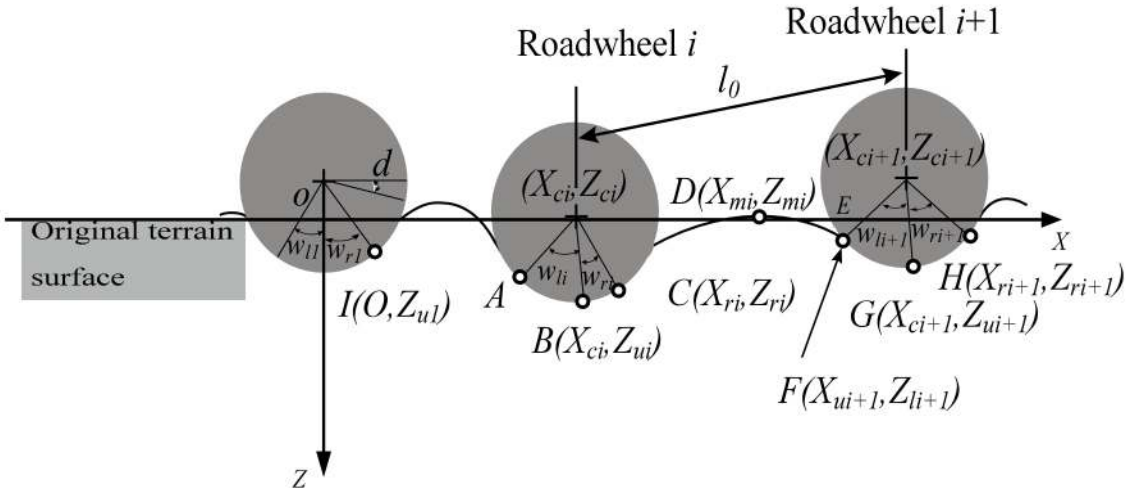
Roadwheel i
Roadwheel i+1
l_0
(X_{ci+1}, Z_{ci+1})
(X_{ci}, Z_{ci})
$D(X_{mi}, Z_{mi})$
E
d
o
Original terrain surface
w_{ll}
w_{rl}
w_{li}
w_{ri}
w_{li+1}
w_{ri+1}
X
$I(O, Z_{ul})$
A
$B(X_{ci}, Z_{ui})$
$C(X_{ri}, Z_{ri})$
$G(X_{ci+1}, Z_{ui+1})$
$H(X_{ri+1}, Z_{ri+1})$
$F(X_{ui+1}, Z_{li+1})$
Z

Fig_5.tif

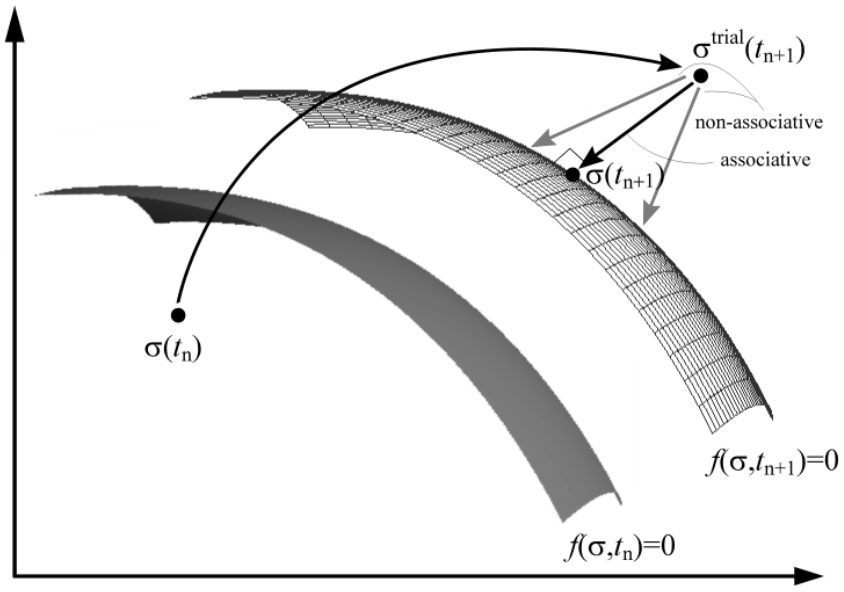
σ^trial(t_n+1)
non-associative
associative
σ(t_n+1)
σ(t_n)
f(σ,t_n+1)=0
f(σ,t_n)=0

Fig_6.tif

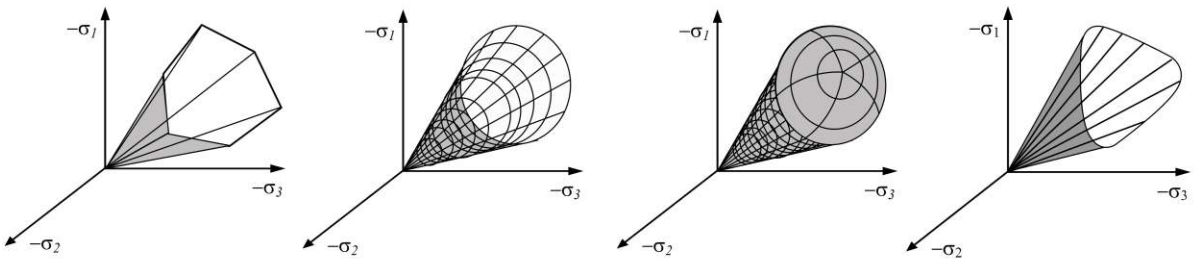

(a) Mohr-Coulomb (b) Drucker-Prager (c) Strain-hardening cap model (d) Lade-Duncan

Fig_7.tif

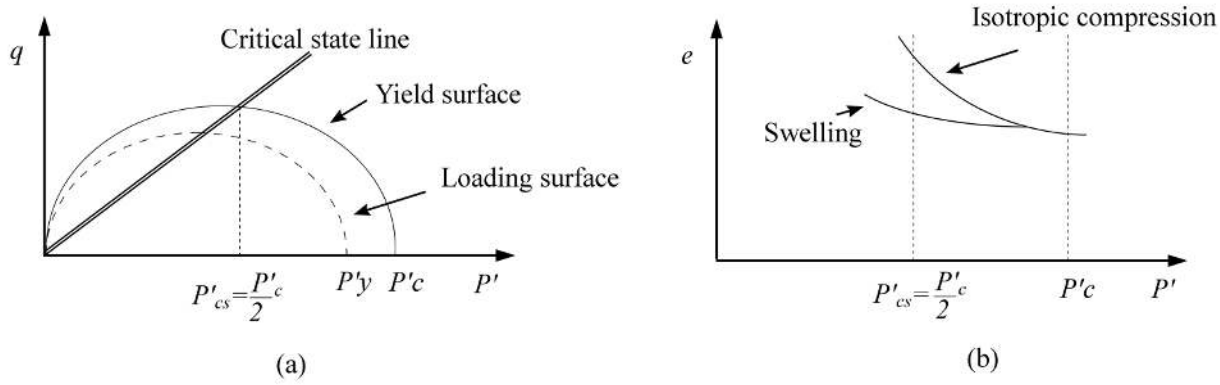
q
Critical state line
Yield surface
Loading surface
P'cs=P'c/2
P'y
P'c
P'
(a)
e
Isotropic compression
Swelling
P'cs=P'c/2
P'c
P'
(b)

Fig_8.tif

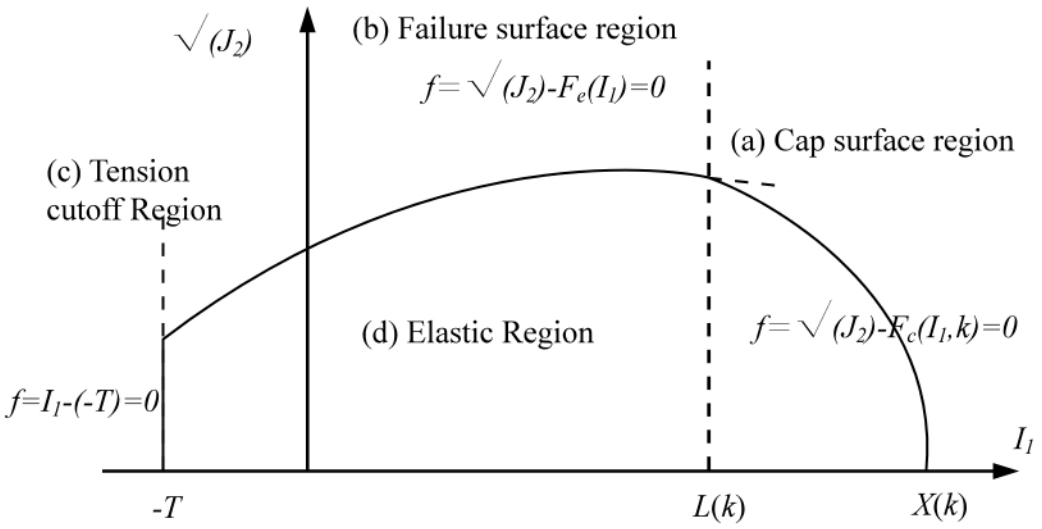
√(J2)
(b) Failure surface region
f=√(J2)-Fe(I1)=0
(a) Cap surface region
(c) Tension
cutoff Region
(d) Elastic Region
f=√(J2)-Fc(I1,k)=0
f=I1-(-T)=0
I1
-T
L(k)
X(k)

Fig_9.tif

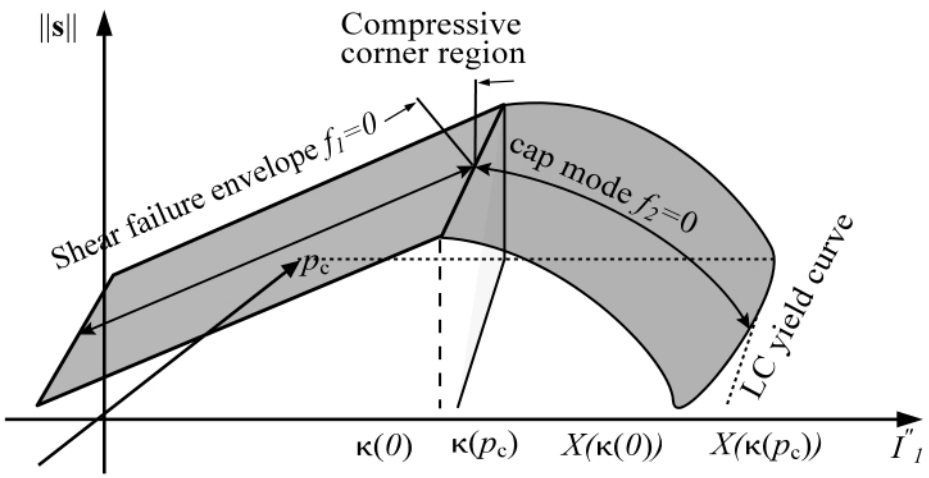
||s||
Compressive
corner region
Shear failure envelope f_1=0
cap mode f_2=0
p_c
LC yield curve
κ(0)
κ(p_c)
X(κ(0))
X(κ(p_c))
I_1

Fig_10.tif

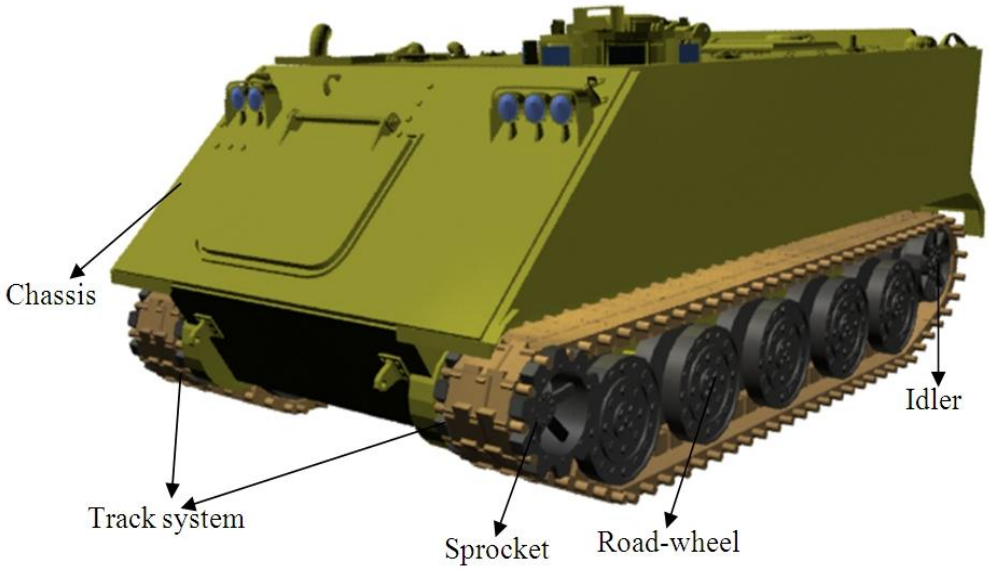

Fig_11.tif